The Astrophysical Journal, 512:874–891, 1999 February 20

X-RAY SPECTROSCOPY OF RAPIDLY ROTATING, LATE-TYPE DWARF STARS

K. P. Singh,[1,2] S. A. Drake,[3,4,5] E. V. Gotthelf,[3,4,6] and N. E. White[3,7]
Received 1998 March 20; accepted 1998 September 28

ABSTRACT

We present an X-ray spectroscopic analysis of two active dwarf stars with extremely short rotation periods, HD 197890 (Speedy Mic) and Gliese 890, using X-ray data acquired with the *ASCA* observatory. We analyze the X-ray spectrum of Speedy Mic in two separate time intervals, one corresponding to an apparent stellar flare, the other to "quiescence" or the nonflaring state. We also present a reanalysis of the *ASCA* spectrum of the M dwarf stellar binary YY Gem, during both quiescent and flaring states. We use the recently updated MEKAL plasma code to model these spectra and find that a minimum of two temperature components are required to obtain good fits for all three stars. The inferred emission measures of the hot components in YY Gem and Speedy Mic, and the temperature of the hot component in the case of YY Gem, increase significantly during the observed X-ray flares, in agreement with previous studies of similar stellar X-ray flares. In addition, metal abundances that are low compared to the solar photospheric values are preferred (but not required) for the quiescent coronae of Gliese 890 and Speedy Mic, while for the quiescent corona of YY Gem, subsolar metal abundances are required and solar abundance models can be ruled out with high confidence. We combine the results of this study with those of previous *ASCA* and *ROSAT* analyses of late-type dwarf stars with known rotation rates to obtain a sample of 17 G, K, and M dwarfs. We find a strong correlation of the X-ray to bolometric luminosity ratio, L_X/L_{bol}, both with the rotation period and the Rossby number (R_o), in agreement with previous studies. Using a homogeneous subset of 10 dwarfs for which we have purely *ASCA*-derived temperatures and elemental abundances, we find that the temperature of the hottest component present in their coronae is correlated with this luminosity ratio, as expected. Finally, we note that the Fe abundances for all active dwarf stars having normalized X-ray luminosities log $(L_X/L_{bol}) > -3.7$ are significantly subsolar, whereas the Fe abundances in the less active stars are within a factor of 2 of the solar value.

Subject headings: stars: abundances — stars: coronae — stars: individual (HD 197890, Gliese 890, YY Geminorum) — X-rays: stars

1. INTRODUCTION

X-ray emission from stars of late spectral type is believed to originate in $10^{6.0}$–$10^{7.5}$ K coronal plasma confined in closed magnetic structures ("loops"). As the stellar rotation speed increases, the dynamo-generated magnetic flux and hence the luminosity and temperature of the coronal plasma increase (Pallavicini et al. 1981). The dynamo activity appears to "saturate" at very high rotation speeds, as has been pointed out in many previous studies, e.g., Rucinski & Vilhu (1983).[8]

Our current knowledge of stellar coronae is based mostly on low spectral resolution X-ray observations carried out with the *Einstein Observatory*, *EXOSAT*, and *ROSAT*. With the launch of the *ASCA* observatory, with its higher spectral resolution over a broader bandpass, a more detailed investigation of the effect of rotation on the physical properties of stellar coronae is now possible. In particular, *ASCA* observations can provide a more sensitive measurement of the coronal plasma temperature structure and prevailing elemental abundances (Singh, White, & Drake 1996). Preliminary studies have included observations of isolated giant stars like β Cet (Drake et al. 1994), subgiant stars in RS CVn–type (White et al. 1994) or Algol-type binaries (Singh, Drake, & White 1995), and a number of active dwarf stars, e.g., the dMe binary star system YY Gem (Gotthelf et al. 1994), the G1.5 V star π^1 UMa (Drake et al. 1994), the K1 V star AB Dor (Mewe et al. 1996), the G0 Ve star EK Dra (Güdel et al. 1997a), and, most recently, the wide visual (G2 V + K1 V) binary system α Cen (Mewe et al. 1998). Analyses of these and other *ASCA* observations have revealed that (1) the coronae in stars with high normalized X-ray luminosities ($L_{X/\mathrm{bol}} \sim -3$, like AR Lac, Algol, AB Dor, and YY Gem, are hotter than those of less active stars ($L_X/L_{bol} \sim -4.5$ to -5.5) in β Cet, Capella, and π^1 UMa, and (2) the metal abundances in active stellar coronae are inferred to be quite different from the solar photospheric values (e.g., Antunes, Nagase, & White 1994; Drake et al. 1994; Gotthelf et al. 1994; White et al. 1994).

We have observed two active single dwarf stars, HD 197890 (SAO 212437) and Gliese 890, as part of an *ASCA* Guest Observer program. HD 197890 first came to notice as a strong and variable extreme-ultraviolet (EUV) source in the *ROSAT* All Sky Survey with the Wide Field Camera (Pounds et al. 1993). Subsequent optical observations found it to be one of the most rapidly rotating single stars discovered so far (Anders et al. 1993; Bromage et al. 1992).

[1] Tata Institute of Fundamental Research, Mumbai 400005, India.
[2] Code 660.2, Laboratory for High Energy Astrophysics, NASA/GSFC, Greenbelt, MD 20771.
[3] Also: Universities Space Research Association, Code 610.3, NASA/GSFC
[4] singh@tifr.res.in.
[5] stephen.drake@gsfc.nasa.gov.
[6] gotthelf@gsfc.nasa.gov.
[7] nicholas.white@gsfc.nasa.gov.
[8] Note that we use the term "saturation" here to describe the observed lack of correlation of X-ray emission with rotation for the most rapidly rotating stars, rather than as a characterization of the underlying physical mechanism responsible for this decoupling: see Solanki, Motamen, & Keppens (1997) for a recent detailed discussion of this issue.

Having a period of only 0.3 days, it was nicknamed "Speedy Mic" by Bromage et al. (1992). The optical and UV characteristics of Speedy Mic based on several photometric and spectroscopic studies can be summarized as (1) a maximum V magnitude V_{max} and corresponding $B-V$ colors of 9.33 and 0.93, respectively (Cutispoto et al. 1997); (2) a spectral type variously estimated to be K0 (Bromage et al. 1992), K3 V (Cutispoto et al. 1997), or K5 (Anders et al. 1993); (3) two possible photometric periods of 9.120 ± 0.096 hr and/or 7.272 ± 0.096 hr (Cutispoto et al. 1997); (4) very broad and strong Ca II H and K emission lines (Matthews et al. 1994); (5) strong Mg II, C II, and C IV ultraviolet emission lines (Robinson et al. 1994); (6) an anomalously high lithium abundance, due to the large 630 mÅ equivalent width of the Li I 6707 Å line; (7) various estimates for the projected rotational velocity $v \sin i$ ranging from 120 ± 20 km s^{-1} (Bromage et al. 1992) through 170 ± 20 km s^{-1} (Anders et al. 1993) to 240 ± 40 km s^{-1} (Matthews et al. 1994); (8) a heliocentric radial velocity v_{rad} of -6.5 km s^{-1} (Bromage et al. 1992); (9) $F_{bol} = 6.5 \times 10^{-9}$ ergs cm^{-2} s^{-1} (Robinson et al. 1994); and (10) a detection in the *ROSAT* All Sky Survey (RASS) at an observed flux level of 4.2×10^{-11} ergs cm^{-2} s^{-1} in the 0.1–2.4 keV energy range. In addition, time-resolved Hα spectroscopy by Jeffries (1993) has shown the presence of transient absorption features, similar to those found for the K dwarf AB Dor, that may be due to corotating clouds of cool material ($N_H \sim 10^{20}$ cm^{-2}) (Anders et al. 1993; Jeffries 1993).

One complication in deriving reliable physical parameters for Speedy Mic has been its uncertain distance, with a value of 40 pc derived by Bromage et al. (1992), based on its hypothesized membership in the Local Association (Pleiades group), and implied status as a young main-sequence star similar to the well-studied K0 dwarf AB Dor, being commonly assumed. Based on its very high rotation speed and high lithium abundance, Anders et al. (1993) suggested that HD 197890 might be a young pre–main-sequence (PMS) object (presumably at a somewhat greater distance) rather than a member of the Pleiades group.

Based on new trigonometric parallax measurements by the *Hipparcos* satellite, the distance to Speedy Mic has now been determined to be $44.4^{+3.5}_{-3.0}$ pc. The implied absolute visual magnitude of 6.1 is then consistent with a spectral type of K2 V in the midrange of most of the prior estimates. The position of Speedy Mic in the observational H-R diagram is also close to the main sequence, supporting its likely status as a young Pleiades-age star. Furthermore, using the new distance measurement, the radial velocity of -6.5 km s^{-1}, and the proper motion of $+0\farcs012$ yr^{-1} in right ascension and $-0\farcs081$ yr^{-1}in declination, we calculate the space velocity components to be $U = -6.0$ km s^{-1}, $V = -17.5$ km s^{-1}, and $W = +0.1$ km s^{-1}. Comparing these values of space motion with Figure 4 of Jeffries (1995), we find that HD 197890 has a space velocity consistent with its membership in the Local Association.

Gliese 890 (=BD $-16°6218$) is an unusual single M dwarf in the solar neighborhood (Gliese 1969), having the second shortest known rotation period P_{rot} of 10.349 hr among M dwarfs (Young, Skumanich, & Harlan 1984a; Young et al. 1984b; Doyle 1987; Young et al. 1990), and consequently a very small value for the Rossby number $R_o = P_{rot}/\tau_c$ (where τ_c is the empirical convective turnover time derived using the Noyes et al. 1984 relation) of 0.016. The optical and UV characteristics of Gliese 890 based on previous photometric and spectroscopic studies are rather similar to those of Speedy Mic, at least those related to activity level, and can be summarized as follows: (1) a V magnitude and a $B-V$ color of 10.8 and 1.40, respectively; (2) a spectral type estimated to be close to dM2e (Joy & Abt 1974 list dM2.5e, while Pettersen et al. 1987 prefer dM1.5e); (3) variable excess emission in the Hα line compared to inactive stars of the same spectral type (Young et al. 1990); (4) strong Mg II, Lyα, and C IV ultraviolet emission lines (Byrne & McKay 1990); (5) a projected rotational velocity $v \sin i$ of ~ 70 km s^{-1} (Young et al. 1984a; Pettersen et al. 1987; Byrne, Eibe, & Rolleston 1996); (6) a heliocentric radial velocity v_{rad} of -6.6 km s^{-1} (Byrne et al. 1996); (7) a stable modulation due to "spots" on its surface, as well as occasional flares, as evidenced from optical photometric data (Young et al. 1984b; Pettersen et al. 1987; Young et al. 1990); (8) evidence from UV and optical observations for the presence of cool "occulting material" at a few stellar radii, variously interpreted as being caused by an "unseen" companion, a circumstellar cloud, and/or large prominence-like features (Byrne & McKay 1990; Doyle & Collier Cameron 1990; Byrne et al. 1996); (9) a parallax for this star as given in the *Hipparcos* catalog of 45.75 ± 2.6 mas, placing it at a distance of 22 ± 1.2 pc; and (10) an *EXOSAT* detection of X-ray emission at a flux level of 8.6×10^{-12} ergs cm^{-2} s^{-1} in the 0.1–4.0 keV energy range, with an estimated coronal temperature of 1.4 ± 0.3 keV (Rao & Singh 1990), and a detection in the RASS at a somewhat lower flux level of 3.0×10^{-12} ergs cm^{-2} s^{-1} in the 0.1–2.4 keV energy range.

Just as for Speedy Mic, it is generally believed that Gliese 890 is a young star of the Pleiades or α Per group age, i.e., 50–70 Myr, which, unlike most other older stars in the solar neighborhood, has not yet lost much of the angular momentum that it gained during its contraction to the main sequence.

Here we present our analysis of data obtained from *ASCA* observations of three late-type dwarf stars, Speedy Mic, Gliese 890, and YY Gem, and our conclusions based on this analysis. The flaring M dwarf system, YY Gem, has been included here because of its similarity in its activity characteristics to the other two stars, with the major difference being that YY Gem is a rapid rotator not because of extreme youth but because it is a tidally-synchronized short-period ($P_{orb} = 0.814$ days) binary system. Although the *ASCA* data on YY Gem were analyzed and presented by Gotthelf et al. (1994), a reanalysis is mandated because of the subsequent updates of the plasma codes, and to enable a proper comparison to be made between the coronal properties of these rather similar stars. The paper is organized as follows: in § 2 we present the details of our *ASCA* observations of Speedy Mic and Gliese 890, in § 3 we give the spectral analysis of the X-ray spectra of the three stars, in § 4 we discuss the inferred coronal temperatures and abundances of these three dwarf stars together with another 14 G–M dwarf stars for which similar data have been obtained, and in § 5 we summarize our conclusions.

2. OBSERVATIONS

2.1. *Speedy Mic*

Speedy Mic was observed with *ASCA* from 1995 April 20, 23:25 UT, to April 21, 12:35 UT, as part of the Guest

Observer program. The *ASCA* observatory (Tanaka et al. 1994), contains four imaging thin-foil grazing incidence X-ray telescopes, two of which are equipped with solid state imaging spectrometers (SISs) and the other two with gas imaging spectrometers (GISs). Each SIS consists of four CCD chips, and each GIS is a gas scintillation proportional counter. The SIS cameras were operated in the 1 CCD mode for these observations with a resultant field of view of $11'.2 \times 11'.2$ and a time resolution of 8 s. The energy resolution of both SISs is about 2% (FWHM) at 5.9 keV, degrading to 6% at 1.0 keV. The GIS data were taken with a time resolution of 62.5 ms. Each GIS has a circular field of view with 20′ radius. The energy resolution of GISs is about 7.8% (FWHM) at 5.9 keV and 19% at 1.0 keV. The energy bandwidth for greater than 10% efficiency is 0.5–10 keV for the SIS and 0.8–10 keV for the GIS.

The observations covered nearly two full rotation periods of the star. The data were selected by applying different criteria for the SIS and the GIS, since the SIS is sensitive to light leakage from the Earth. For the SIS, the data were selected when the telescope viewing direction was more than 25° from the bright Earth limb and more than 10° from the dark Earth, while the GIS data were selected for the periods when the Earth elevation angle was greater than 10°. These selections resulted in useful exposure times of $\sim$22,820 s and $\sim$28,450 s in the SIS and GIS detectors, respectively. Hot and flickering pixels in the CCDs were eliminated using the FTOOLs task CLEANSIS, which rejects all the pixels that do not follow Poissonian statistics (see Day et al. 1995 for details). The counts and pulse height spectra were accumulated from a source region of 4′ radius in the SIS and 6′ radius in the GIS, while the background was taken from source-free regions in the SIS and GIS where counts from the outer wings of the point–spread function of the source were minimized. An X-ray light curve of Speedy Mic in the 0.4–10 keV energy band obtained by combining the SIS0 and SIS1 data is presented in Figure 1. X-ray emission from Speedy Mic was detected with an average count rate of $\sim$0.14 counts s^{-1} above background in SIS detectors and 0.06 counts s^{-1} in GIS detectors. The source was found to be steady for most of the observation, except near the end, when it increased in its intensity by factor of $\sim$2, and stayed at that level for $\sim$2000 s. No evidence of rotational modulation at the period of about 7 hr seen in the optical is found in the X-ray emission. Henceforth, we shall refer to the last hour of the X-ray light curve as a "flare" and the rest as being in a "quiescence" state. The average X-ray flux observed in the 0.5–10 keV energy band was 3.7×10^{-12} ergs cm^{-2} s^{-1}, which implies an X-ray luminosity of 8.7×10^{29} ergs s^{-1} during the "quiescence." The average X-ray flux during the "flare" was 7.9×10^{-12} ergs cm^{-2} s^{-1}. The flux estimates are based on the best-fit spectral models in § 3.

Apart from Speedy Mic, three new X-ray sources were also detected in the fields of view of the GIS2 and GIS3 detectors. The positions and count rates detected in GIS2 from these sources are given in Table 1. These sources are factors of 5–10 weaker than Speedy Mic in the quiescent state and well resolved and separated from Speedy Mic. These three sources are also detected in a deep pointing observation with the higher resolution *ROSAT* Position

TABLE 1

NEW SOURCES DETECTED WITH *ASCA* GIS

Source Number	Instrument	R.A.(2000)	Decl.(2000)	Count Rate[a] (counts s^{-1})
1	GIS2	20 48 07.6	−36 26 47.6	0.0070 ± 0.0009
	PSPC	20 48 11.0	−36 26 32.7	0.0138 ± 0.0008
2	GIS2	20 47 13.7	−36 28 13.7	0.0040 ± 0.0008
	PSPC	20 47 14.0	−36 28 08.6	0.0013 ± 0.0003
3	GIS2	20 47 29.3	−36 13 58.1	0.0110 ± 0.0010
	PSPC	20 47 31.8	−36 13 37.8	0.0633 ± 0.0020
4	GIS2	23 07 48.4	−15 31 32.8	0.0070 ± 0.0008
	PSPC	23 07 51.5	−15 32 09.1	0.0114 ± 0.0018
5	GIS2	23 07 31.1	−15 26 34.5	0.0060 ± 0.0009
	PSPC	23 07 34.4	−15 26 53.4	0.0180 ± 0.0023

NOTE.—Units of right ascension are hours, minutes, and seconds, and units of declination are degrees, arcminutes, and arcseconds.

[a] After background subtraction.

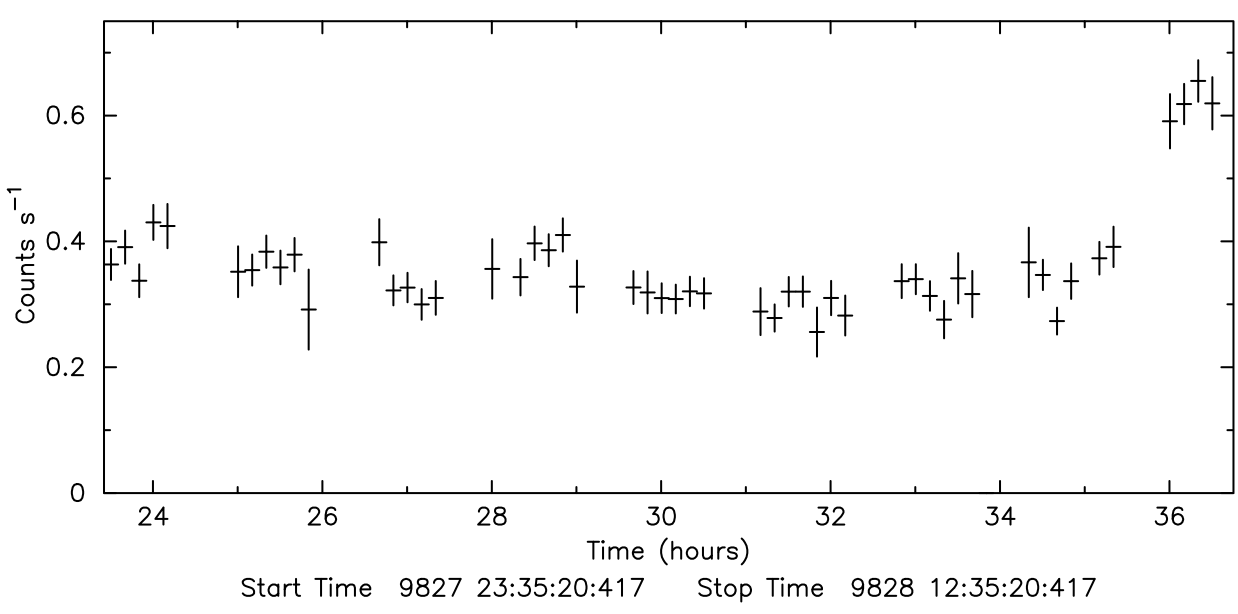

FIG. 1.—Combined SIS0 and SIS1 X-ray light curve of Speedy Mic

Sensitive Proportional Counter (PSPC). The PSPC-determined positions of these new sources, and their total PSPC count rates are also given in Table 1. Although the PSPC pointed-mode observation of Speedy Mic detected many sources ($\simeq 28$) other than Speedy Mic in its large field of view, Speedy Mic is the brightest, and there are only three other, very weak sources within the *ASCA*-determined error circle centered on its position, with a total contribution of only $\sim 1\%$ of the observed PSPC count rate of Speedy Mic itself. Thus, it is unlikely that the *ASCA* spectrum of Speedy Mic is significantly contaminated by these other nearby sources.

2.2. *Gliese 890*

Gliese 890 was observed with *ASCA* from 1995 November 18, 09:29 UT, to November 19, 12:20 UT, as part of the Guest Observer program. Following the same selection criterion as in the case of Speedy Mic, observations resulted in useful exposure times of $\sim 24{,}000$ and $\sim 27{,}900$ s in the SIS and GIS detectors, respectively. The counts and pulse–height spectra were accumulated from source and background region in the same manner as above. X-ray emission from Gliese 890 was detected with an average count rate of ~ 0.087 counts s^{-1} above background in SIS detectors, and 0.046 counts s^{-1} in GIS detectors. An X-ray light curve of Gliese 890 in the 0.5–10 keV energy band obtained by combining the SIS0 and SIS1 data is presented in Figure 2. The source was found to be fairly steady for most of the observation, except near the end, when it shows a large flarelike event with the intensity going up by a factor of ~ 2, and then decaying almost exponentially on a timescale of about 2400 s. No evidence of rotational modulation at the period of about 10.3 hr seen in the optical is found in the X-ray emission. The average X-ray flux observed in the 0.5–10 keV energy band was 3.0×10^{-12} ergs cm^{-2} s^{-1}, which implies an average X-ray luminosity of 1.74×10^{29} ergs s^{-1}. The flux estimates are based on the best-fit spectral models in § 3. The X-ray emission from Gliese 890 is thus fainter by a factor of ~ 3 in the present observations when compared to its brightness observed with *EXOSAT* 10 years ago (Rao & Singh 1990).

Two new X-ray sources, other than Gliese 890 and well separated from it, were also detected with the GIS2 and GIS3 detectors. The positions and count rates detected from these sources are given in Table 1. These sources are factors of 6–7 weaker than Gliese 890. We have also examined the higher resolution soft X-ray images obtained with *ROSAT* PSPC and find that the two new sources are detected in those observations as well. The PSPC-determined positions of these new sources and their total count rates in PSPC are also given in Table 1. There are no sources other than Gliese 890 within the *ASCA* determined error circle of Gliese 890, and therefore there is no confusion.

2.3. *YY Gem*

The details of *ASCA* observations of YY Gem have been given by Gotthelf et al. (1994). An X-ray flare was also detected from YY Gem, and the X-ray spectra during the flare and quiescence have been reextracted for a joint fit to the data from all the detectors.

3. SPECTRAL ANALYSIS AND RESULTS

We have analyzed the SIS data for $E > 0.5$ keV and the GIS data for $E > 0.65$ keV. Furthermore, the data were grouped so as to have a minimum of 20 counts per energy channel. Due to the weakness of the sources, data from similar detectors like SIS0 and SIS1 were combined, as were the data from the GIS2 and GIS3 detectors, prior to the analysis.

The SIS and GIS spectra were analyzed jointly using the XSPEC version 10.0 software (Arnaud 1996). We used the latest version of the coronal plasma emission code known as MEKAL (Mewe, Kaastra, & Liedahl 1995) and VMEKAL, i.e., MEKAL with variable abundances for individual elements. These plasma emission models incorporate the Liedahl, Osterheld, & Goldstein (1995) updates to the Fe L line strengths in the older version MEKA (Kaastra & Mewe 1993). The Fe L complex dominates coronal spectra at energies near 1 keV, and, despite these recent updates, it is undoubtedly true that the current knowledge of both the number of and the atomic data for the myriad emission lines in this spectral region is still quite incomplete (see Brickhouse et al. 1997). To fit the *ASCA* spectra, we have

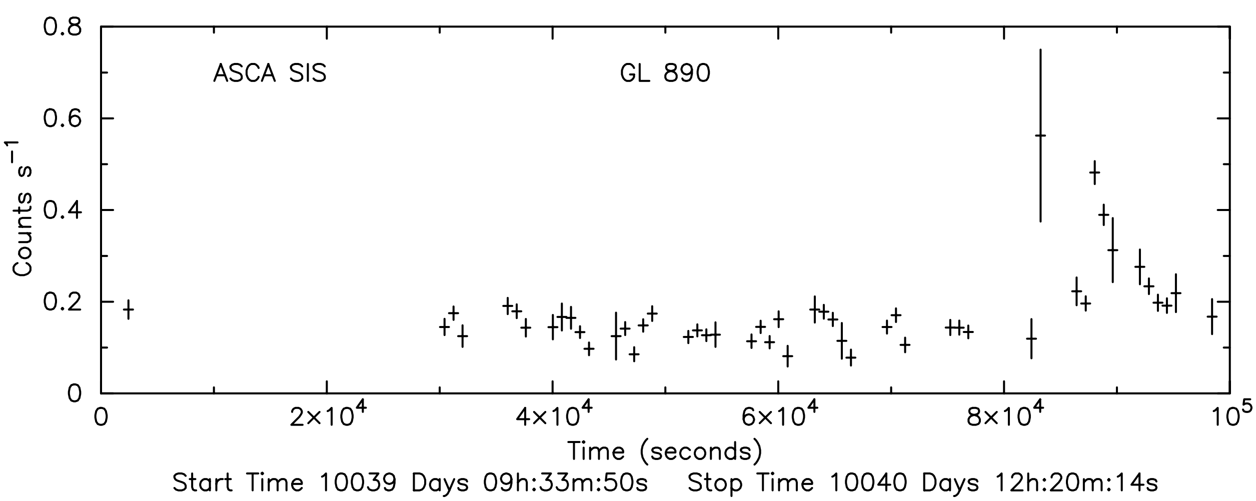

FIG. 2.—Combined SIS0 and SIS1 X-ray light curve of Gliese 890. The bin time is 800 s.

tried a variety of different models: (*a*) a single-temperature plasma model, (*b*) a model consisting of two or more discrete plasma components at different temperatures; and (*c*) a continuous emission measure (CEM) plasma model based on a representation of the distribution of emission measure as a function of temperature by Chebyshev polynomials of the 6th order (used on the higher statistical quality data obtained during quiescence). Such models have been described in Lemen et al. (1989) and have been used recently by Singh et al. (1996), and Kaastra et al. (1996). The elemental abundances in the plasma for the models could be varied with respect to the solar photospheric values taken from Anders & Grevesse (1989).

3.1. *Speedy Mic*

We have extracted and analyzed the spectral data for the quiescent and flaring states, separately. The SIS and GIS spectra are shown in Figures 3 and 4 for the quiescent and flare states, respectively. The higher resolution SIS spectra show little evidence for discrete lines such as the resonance lines of the He-like and H-like ions of Mg, Si, and S at 1.4, 1.9, and 2.5 keV, respectively, but are dominated by the broad and essentially unresolved hump of the Fe L-shell complex centered at ∼0.9 keV together with a fairly featureless higher energy "continuum" emission that is detected up to energies ∼6 keV. The SIS spectra in the two states, when compared by taking their ratios and plotted in Figure 5, indicated the presence of spectral hardening associated with the increased brightness during the flare.

The results based on the present analyses of the quiescent and flaring states of Speedy Mic are given in Table 2. Single-temperature models are found to be statistically unacceptable (i.e., to have reduced χ^2 values, χ^2_ν, in excess of 1.15 [1.24] for 145 [60] degrees of freedom [dof], which can be rejected at the 90% confidence level), and results based on such single-temperature models are not listed here. By the same criterion, two-temperature models with solar photospheric abundances were found to be unacceptable for the quiescent state but acceptable for the flaring state. CEM models with solar abundances give acceptable fits to both the quiescent and the flaring state spectra. A significant improvement in the fit to the quiescent spectrum was found using nonsolar abundances rather than fixed solar abundances (see Table 2), based on the value of $\Delta\chi^2$ (≥ 50) and the *F*-statistic, for two-temperature as well as CEM models. Using the MEKAL model, and varying the abundances of all the elements together, results in a very good fit to the data in both the quiescent and the flaring states. The overall abundance value of ∼0.2 solar for all the elements is about the same during the quiescence and the flare. In the quiescent state, a further significant improvement ($\Delta\chi^2 \geq 25$) in the fit is obtained using a two-temperature VMEKAL model in which the abundances of O, Mg, Si, S, and Fe are allowed to vary individually; because of the large formal uncertainty in the Ne abundance value that was obtained when it was allowed to vary (due presumably to the confusion of the strongest Ne X emission lines within the Fe L emission-line complex at the resolution of the *ASCA* detectors), the Ne abundance was left fixed at its solar value. Because of the low signal-to-

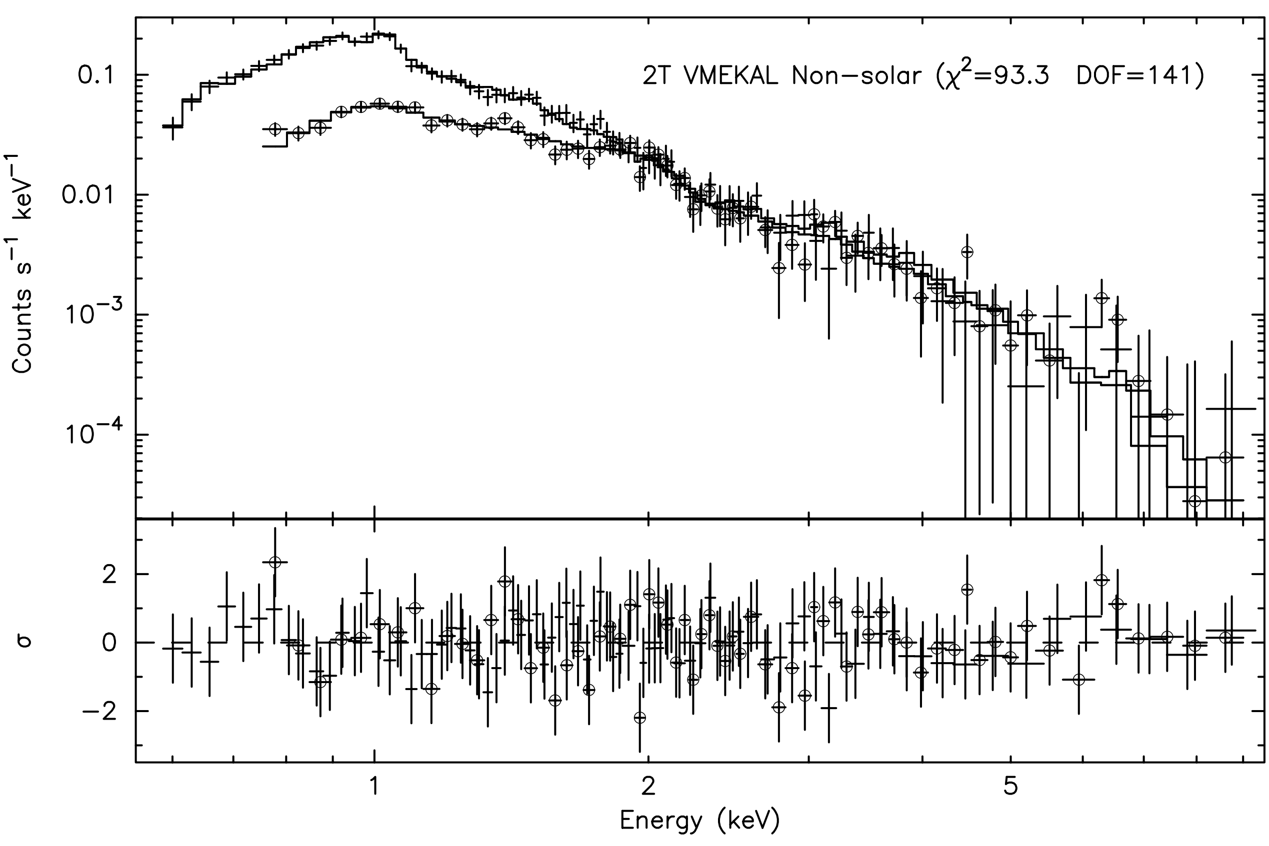

FIG. 3.—X-ray spectrum of Speedy Mic in its quiescence state. Combined data from SIS0 and SIS1 are shown with plus signs, and the combined data from GIS2 and GIS3 are marked with circles. The best-fit two-temperature plasma model fitted jointly to both sets of data is shown as histograms. The bottom panel shows the significance of the residuals in terms of their σ-values.

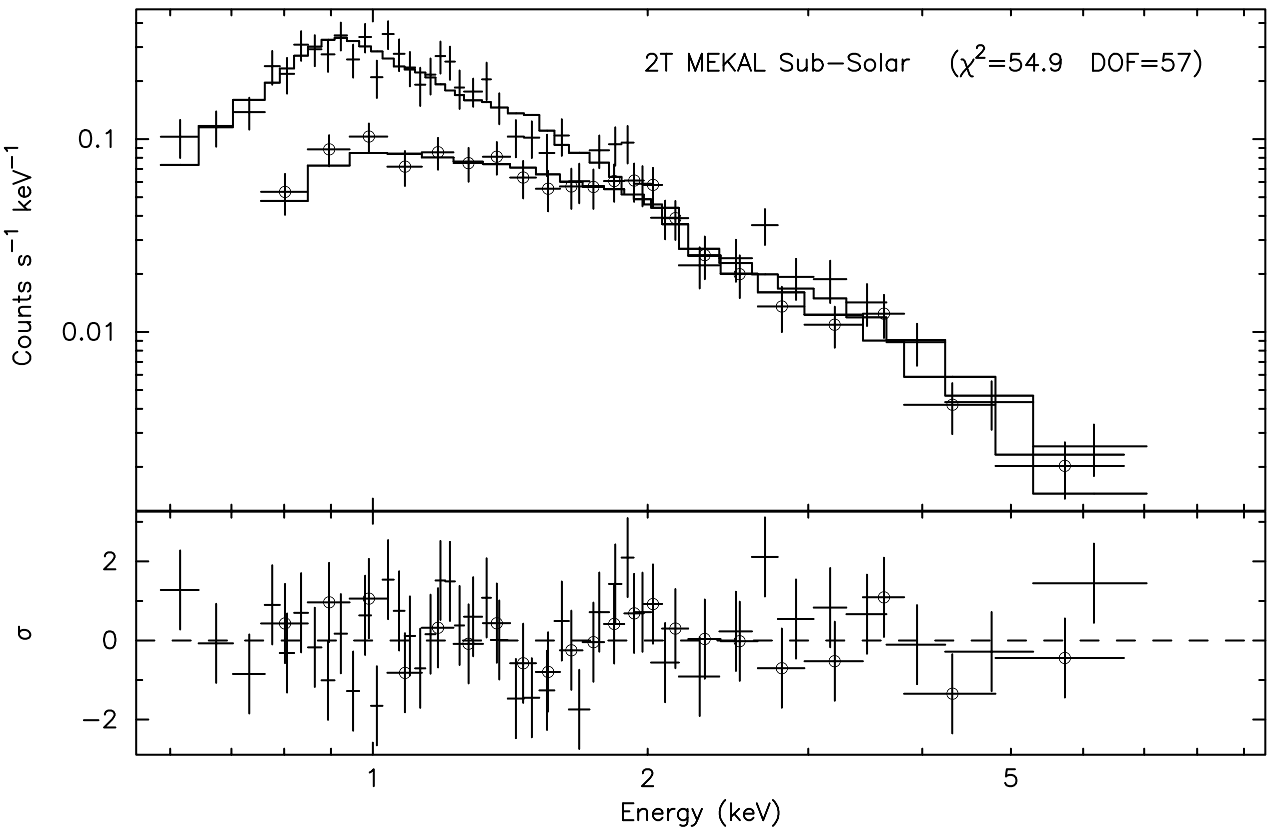

FIG. 4.—Same as Fig. 3, but for the X-ray " flare " from Speedy Mic

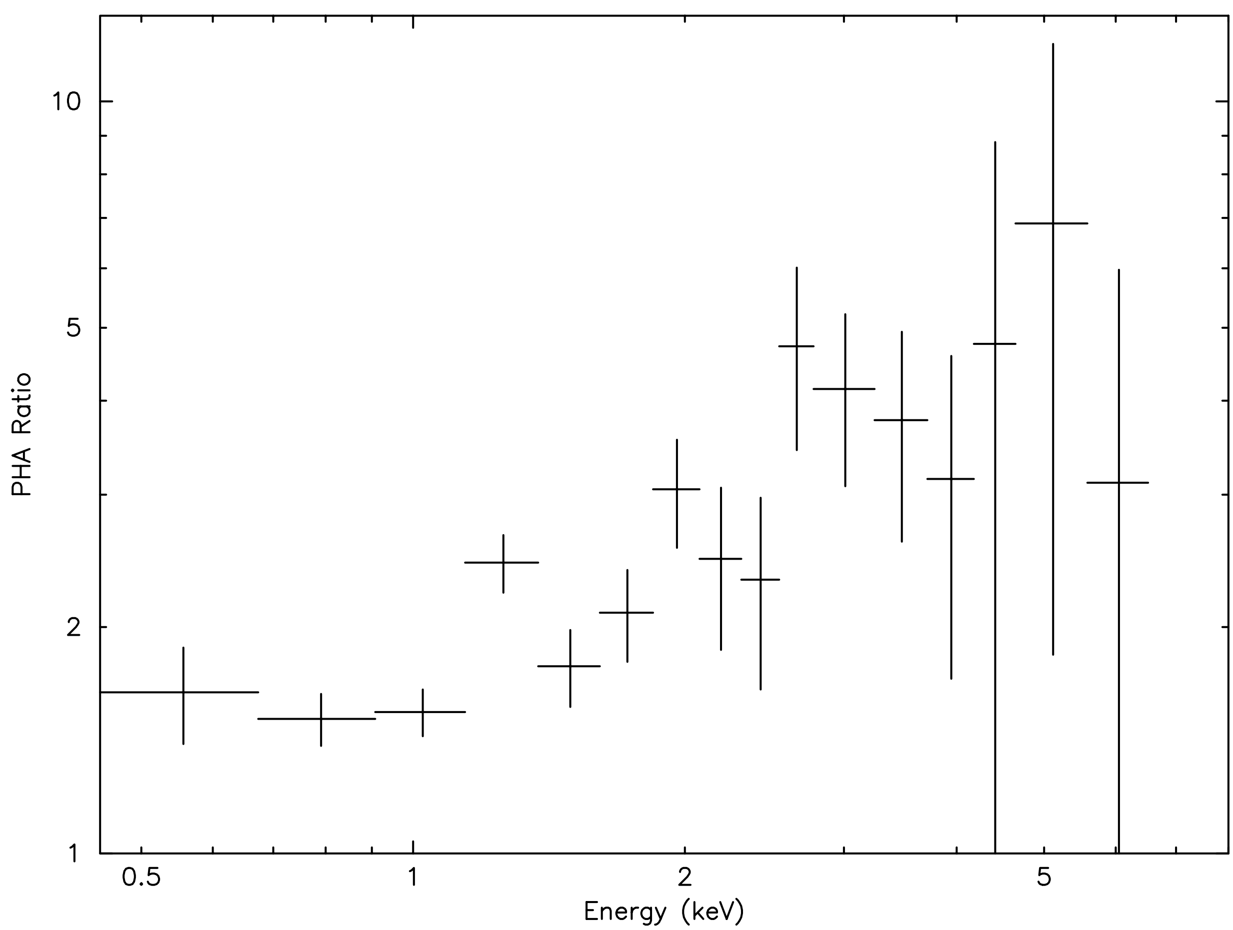

FIG. 5.—Ratio of pulse-height analyzer (PHA) data of the " flare " spectrum to the " quiescent " spectrum

TABLE 2

RESULTS FROM JOINT ANALYSIS OF SIS AND GIS SPECTRA OF SPEEDY MIC

Abundances Relative to Solar Photospheric[a]	kT (keV)	Emission Measure (10^{52} cm^{-3})	χ^2	Degrees of Freedom
Two-Temperature Models during Quiescence				
1.0 (fixed)	$(0.68^{+0.02}_{-0.02}, 2.5 \pm 0.2)$	$(1.27 \pm 0.07, 3.7 \pm 0.2)$	170.8	146
$0.18^{+0.08}_{-0.11}$	$(0.77 \pm 0.05, 2.1^{+6.0}_{-0.3})$	$(6.2^{+8.5}_{-1.9}, 4.7^{+0.5}_{-3.1})$	120.5	145
$(O=0.5^{+0.4}_{-0.2}$, $Mg=0.3^{+0.22}_{-0.25}$, $Si=0.34^{+0.20}_{-0.18}$, $S<0.70$, $Fe=0.21^{+0.08}_{-0.06})$	$(0.65 \pm 0.05, 2.2^{+0.6}_{-0.3})$	$(4.0^{+1.1}_{-0.8}, 4.3 \pm 0.6)$	93.3	141
Continuous Emission Measure Models during Quiescence				
1.0 (fixed)	[b]	[b]	140.9	144
0.21 ± 0.06	[b]	[b]	95.05	143
Two-Temperature Models during Flare				
1.0 (fixed)	$(0.70^{+0.09}_{-0.06}, 3.5 \pm 0.5)$	$(1.6^{+0.4}_{-0.2}, 9.5^{+0.8}_{-0.9})$	61.5	58
$0.23^{+0.40}_{-0.17}$	$(0.74^{+0.11}_{-0.09}, 3.2^{+2.3}_{-0.5})$	$(6.1^{+12}_{-3.7}, 11.8^{+2.0}_{-3.8})$	54.8	57

NOTE—Errors and upper limits are with 90% confidence based on $\chi^2_{min} + 2.71$; distance = 44.4 pc.

[a] Common value of abundances for all the elements in the code, except where stated otherwise.

[b] Sixth-order Chebyshev polynomial.

noise ratio of the flaring state spectrum of Speedy Mic, and the good fits already obtained with simpler models, we did not attempt a multiabundance (VMEKAL) fit in this case.

The best-fit two-temperature nonsolar abundance model (VMEKAL) for the quiescent state is shown plotted as a histogram in Figure 3, along with the data, while the best-fit two-temperature nonsolar abundance model (MEKAL) for the flaring state is shown plotted as a histogram in Figure 4. A significant increase in the emission measure of the high-T component is observed during the flare as compared to the quiescent state (see Table 2). This increase is independent of the abundances used in the models. An increase in the temperature of the hotter component is indicated when variable abundances are used. This increase is, however, significant only if solar abundance values are used. We have derived the 68%, 90%, and 99% confidence regions for the emission measures and temperatures that fit the quiescent and flaring spectra of Speedy Mic, for both solar abundance and nonsolar models. For the nonsolar MEKAL models where all the metal abundances were allowed to vary by the same factor, these confidence regions are shown as contour diagrams in Figures 6*a* and 6*b*. (We do not show the confidence diagrams for the solar abundance models, since their fit to the Speedy Mic quiescent spectrum was not formally acceptable.)

The best-fit CEM models, shown in Figure 7, have a differential emission measure (DEM) distribution showing two peaks, in agreement with our finding that models with two discrete temperature components can yield good fits to the observed spectra.

3.2. *Gliese 890*

The source is weaker than Speedy Mic, and the counts are insufficient to analyze the quiescent and flare spectra separately. We therefore accumulated an average spectrum, combining the individual spectra from the two SIS detectors, SIS0 and SIS1, as well as combining the spectra from the two GIS detectors, GIS2 and GIS3. The combined SIS

TABLE 3

RESULTS FROM JOINT ANALYSIS OF SIS AND GIS SPECTRA OF GLIESE 890

Abundances Relative to Solar Photospheric[a]	kT (keV)	Emission Measure (10^{52} cm^{-3})	χ^2	Degrees of Freedom
One-Temperature Models				
1.0 (fixed)	0.88	0.35	384.7	154
0.066 ± 0.015	$0.80^{+0.05}_{-0.05}$	$2.4^{+0.4}_{-0.3}$	81.4	152
Two-Temperature Models				
1.0 (fixed)	$(0.70^{+0.04}_{-0.03}, 2.8^{+0.6}_{-0.5})$	$(0.21 \pm 0.02, 0.45^{+0.05}_{-0.04})$	106.8	151
$0.084^{+0.02}_{-0.02}$	$(0.77 \pm 0.04, >2.0)$	$(1.9^{+0.4}_{-0.3}, 0.20^{+0.08}_{-0.09})$	67.8	150
Continuous Emission Measure Models				
1.0 (fixed)	[b]	[b]	96.9	148
0.20 ± 0.14	[b]	[b]	76.4	147

NOTE.—Errors and upper limits are with 90% confidence based on $\chi^2_{min} + 2.71$; distance = 22 pc.

[a] Common value of abundances for all the elements in the code, except where stated otherwise.

[b] Sixth-order Chebyshev polynomial.

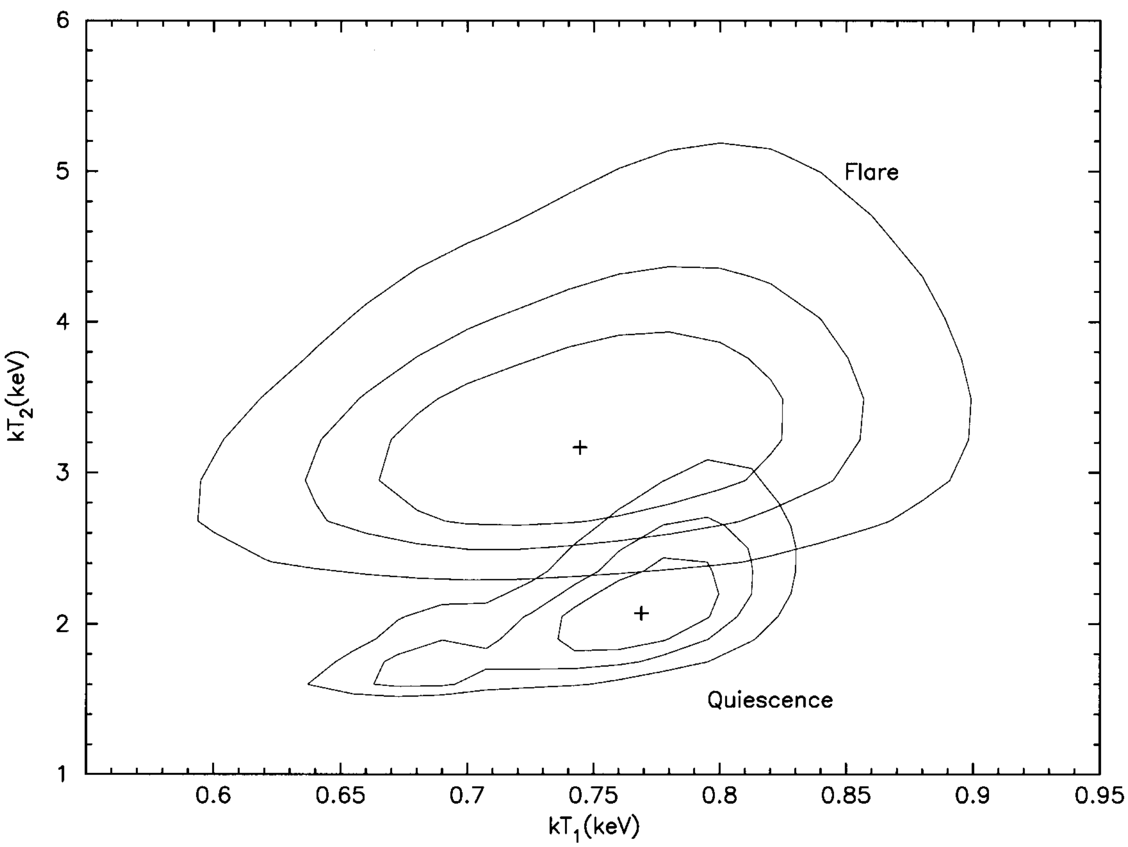

FIG. 6*a*

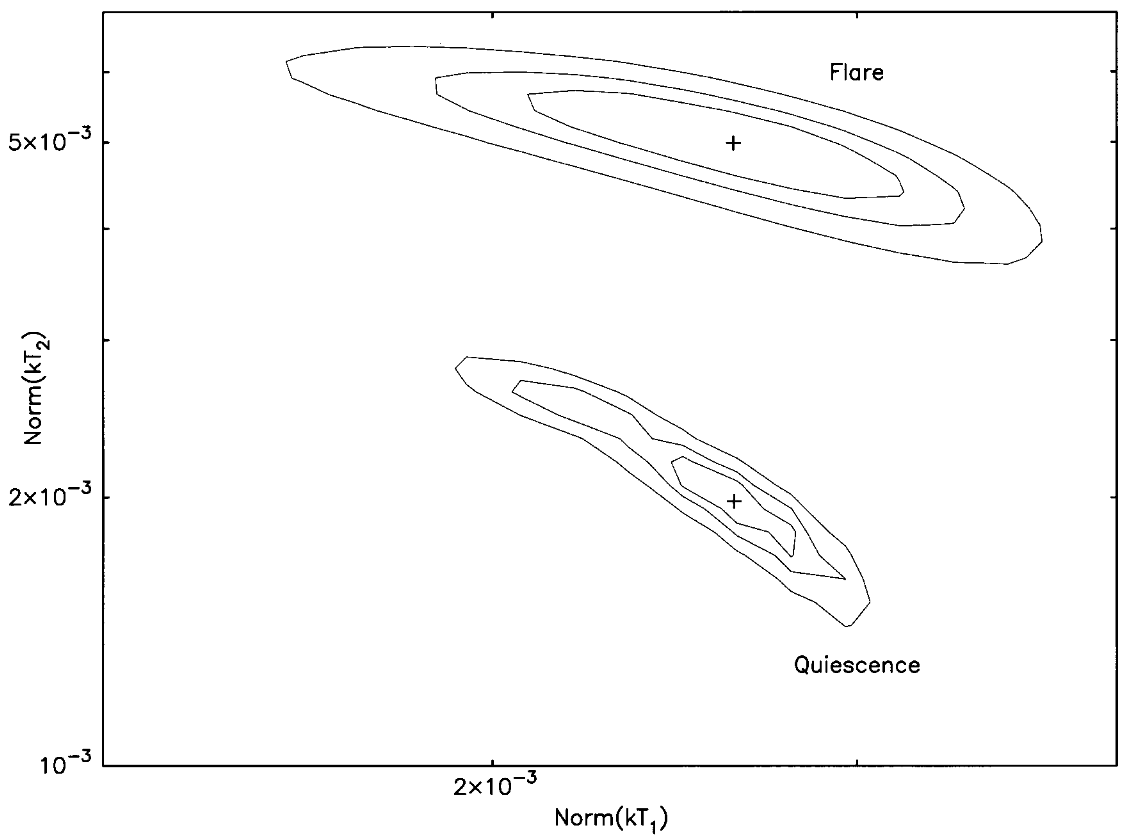

FIG. 6*b*

FIG. 6.—Allowed ranges of (*a*) the two temperatures and (*b*) the emission measures corresponding to the two temperatures, in the X-ray spectrum of Speedy Mic for 68%, 90%, and 99% confidence based on counting statistics. The abundances of all the elements were allowed to vary together. The emission measures (or norms) are in units of $1.2 \times 10^{52} d_{pc}$ cm^{-3}, where d_{pc} is 40 pc for Speedy Mic. Both quiescent and flare states are shown.

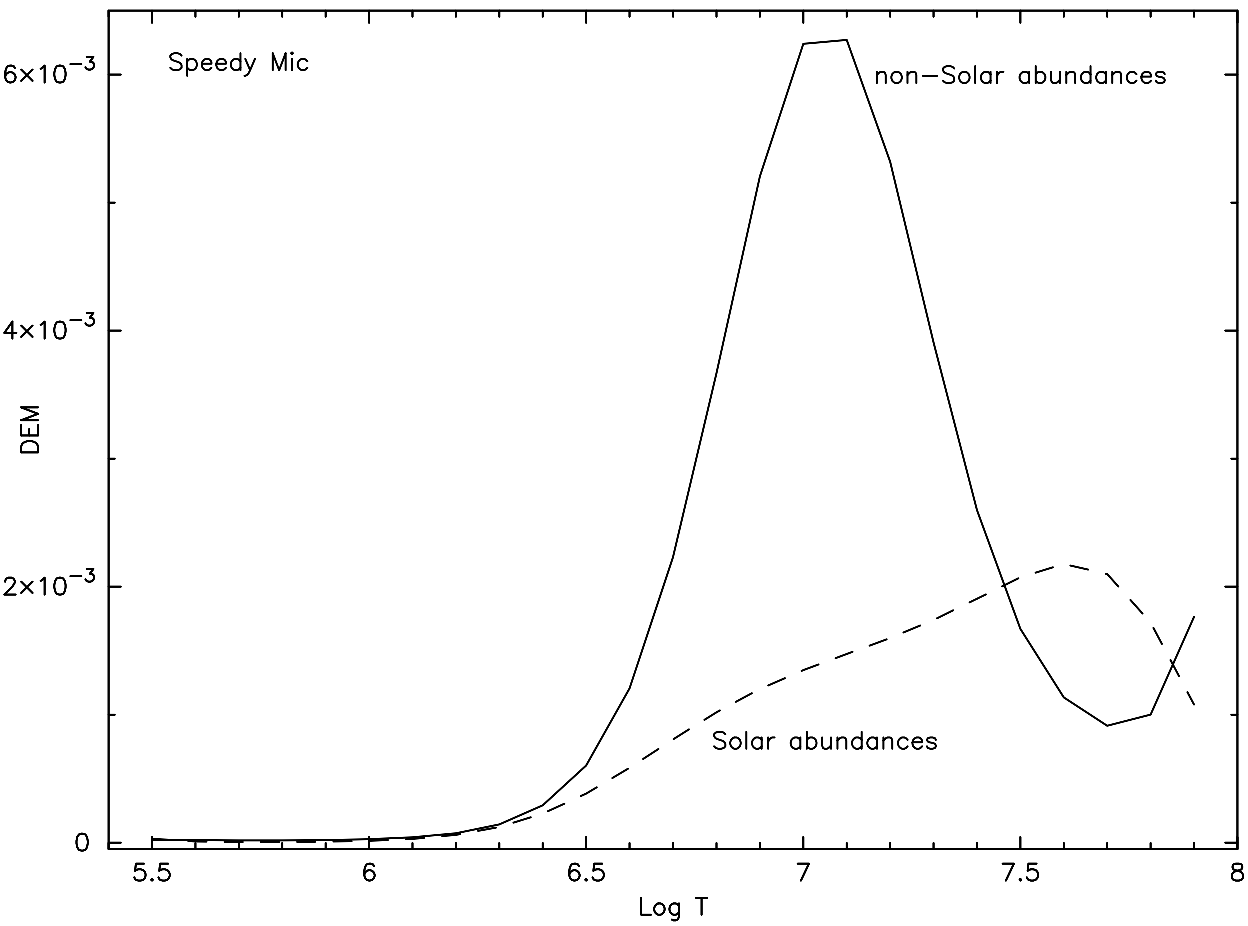

FIG. 7.—Differential emission measure derived using the sixth-order Chebyshev polynomials plotted in units of 1.2×10^{52} ergs s^{-1} $d_{\rm pc}^2$ for Speedy Mic. The best-fit distributions for both the solar and nonsolar abundance models are shown.

and GIS spectra are displayed in Figure 8, and were analyzed jointly in the same fashion as before. The results based on the present analyses of Gliese 890 are given in Table 3. Single-temperature models with solar abundance are rejected as $\chi_\nu^2 > 2.0$. Allowing the abundance to be a free parameter in the fit, however, gives a much better fit to the data for highly subsolar abundances, although large residuals both at low (<1 keV) and high (>3 keV) energies can still be seen. Two-temperature and CEM models with solar photospheric abundances are found to give statistically acceptable fits to the data. Allowing the abundances of all the elements to vary together results in a statistically improved fit to the data with $\Delta\chi^2 > 20$ for an overall abundance value in the range of 0.06–0.30 solar. The best-fit two-temperature nonsolar abundance model (MEKAL) is shown plotted as a histogram in Figure 8, along with the data. The best-fit CEM models are shown in Figure 9 and exhibit a double-peaked DEM distribution. The poor signal-to-noise ratio in the spectra of Gliese 890 does not warrant the use of VMEKAL models.

3.3. *YY Gem*

The *ASCA* spectrum of YY Gem obtained from just one detector, SIS0, was analyzed by Gotthelf et al. (1994). Here, we present a reanalysis of the data from all of the four detectors aboard *ASCA*. Our reanalysis also uses the updated versions of the plasma codes, i.e., MEKAL and VMEKAL as opposed to the MEKA model used in the original analysis. As for the other two stars, the combined SIS and GIS data were analyzed jointly. The results of our analysis for the quiescent and flaring states of YY Gem are presented in Table 4. The SIS and GIS spectra of YY Gem in the quiescent state are shown in Figure 10.

For solar abundance models, the overall fit to the spectra during quiescence was found to improve by going from two to four discrete temperature components. Beyond the four-temperature model, however, there was no further improvement. For $\simeq 230$ dof, models with a $\chi_\nu^2 \geq 1.12$ are not acceptable at the 90% confidence level. By this criterion, two-, three-, and four-temperature and even CEM models with solar abundances are not acceptable, as they result in minimum $\chi_\nu^2 > 1.12$. The spectrum predicted for the best-fit solar abundance four-temperature model is shown as a histogram in Figure 10, together with the observed spectrum. Finally, the DEM distribution for the best-fit (solar and nonsolar) CEM models are shown in Figure 11. As in the case of Speedy Mic, the CEM models for YY Gem also have a double-peaked distribution, reminiscent of the two-temperature discrete temperature structure.

Allowing the abundances of the metals in the plasma model to vary has a dramatic effect in improving the fit to the data, as reflected in the value of $\Delta\chi^2$ (>100) and the *F*-statistic. The MEKAL models in which all the metal abundances are varied by a single common value and that give an acceptable fit to the data require at least three discrete temperature components and an overall metal abun-

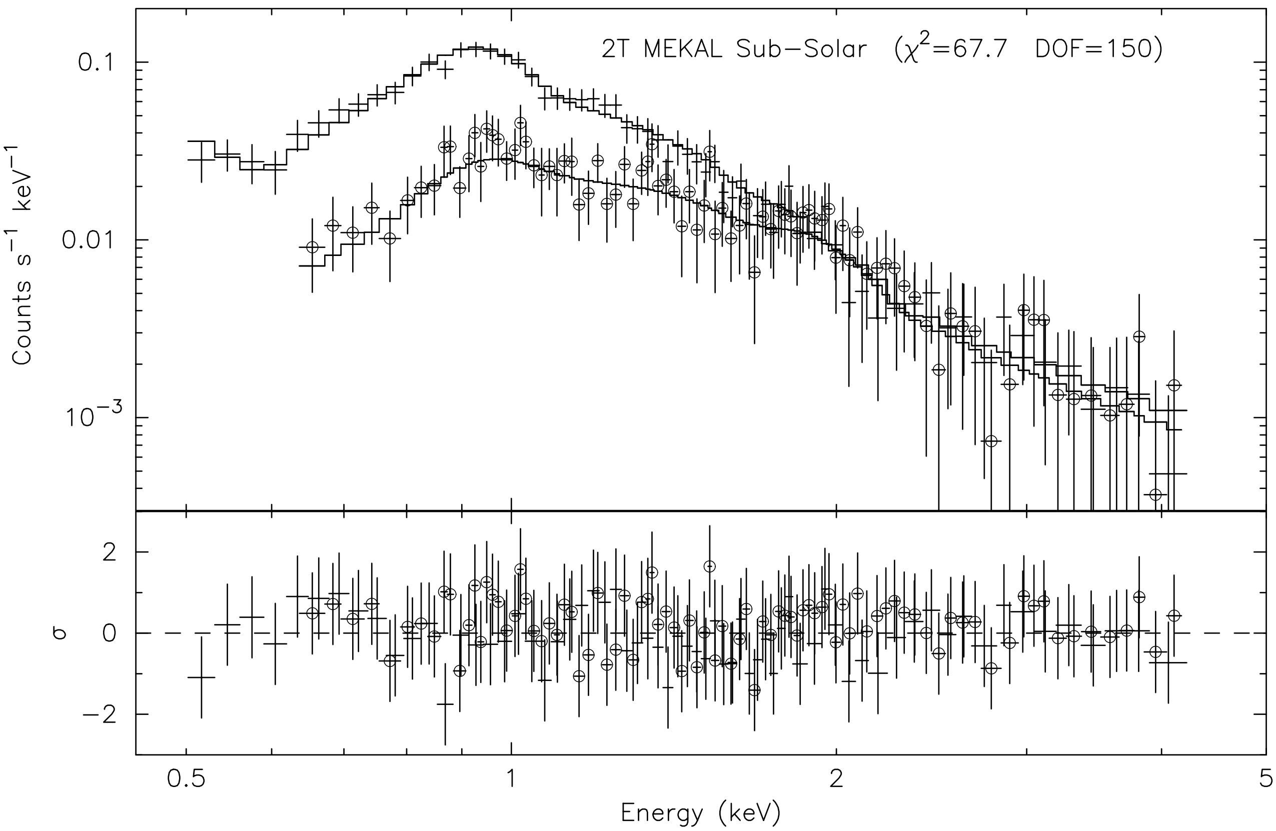

FIG. 8.—X-ray spectrum of Gliese 890. Combined data from SIS0 and SIS1 are shown with plus signs. and the combined data from GIS2 and GIS3 are marked with circles. The best-fit two-temperature plasma model fitted jointly to the two sets of data is shown as histograms. The bottom panel shows the significance of the residuals in terms of their σ-values.

dance in the range of $\sim$0.2–0.3 times the solar photospheric value. However, an even better fit to the spectrum can be achieved by varying the abundances of the individual elements (i.e., using the VMEKAL model) for a model having only two discrete temperature components. Adding a third component in this case leads to only marginal improvement. The spectrum of the best-fit two-temperature model with individually variable abundances for O, Mg, Si, S, Ar, Ca, and Fe is shown as a histogram in Figure 12.

For the X-ray spectra of the flaring state of YY Gem, acceptable fits are found with both the solar and nonsolar abundance models with just two temperature components. The addition of a third temperature component does, however, significantly improve the fit. In contrast, varying the overall abundance value leads to only a marginal improvement in the fit. The best-fit abundance value is in the range of 0.42–0.81 times the solar value with 90% confidence using the three-temperature model during the flare. To judge the significance of higher abundance during the flare, we tried using the fixed abundance value of 0.60 times solar for the quiescent data. The χ^2_ν values for the two-, three-, and four-temperature and CEM models are 1.99, 1.204, 1.17, and 1.415 respectively, thus ruling out such a high value of the abundance for the quiescent spectra. The increase in the abundance during the flare is, therefore, significant at the 90% confidence level. The signal-to-noise ratio in the flare spectrum is, however, not good enough to justify varying the abundances of the elements individually. The emission measure of the highest temperature in YY Gem also increases significantly during the flare. There is, however, only marginal evidence for an increase in the temperature of this component during the flare.

4. DISCUSSION

4.1. *Temperatures*

We find that the X-ray spectra of both Speedy Mic and Gliese 890 show a significant hard component ($kT \simeq$ 2–3 keV), which is similar to the one found in YY Gem. The presence of such a hard component, which is absent from the spectrum of less active ($L_X/L_{bol} \sim 10^{-5}$) stars such as π^1 UMa, β Cet, and Capella, appears to be a signature of stars whose coronae are exceptionally active ($L_X/L_{bol} \sim 10^{-3}$), such as these three dwarfs and the RS CVn and Algol binary systems.

Both the emission measure and the temperature of the highest temperature component in the spectrum of YY Gem increase significantly during the flares, by factors of 5.5 and 1.5, respectively, for the three-temperature scaled solar abundance model appropriate for its spectrum. A similar trend also appears to be present in Speedy Mic, with the emission measure and temperature increasing by factors of 2.6 and 1.5, respectively, for the two-temperature scaled solar abundance model. It should be noted that in the case of YY Gem, although the emission measure of the 2.8 keV component dominates the X-ray emission during the flare, that of the lowest temperature ($\sim$0.3 keV) component during the flare was lower than during the quiescent period, perhaps making the association of the low-temperature component with YY Gem more plausible than its associ-

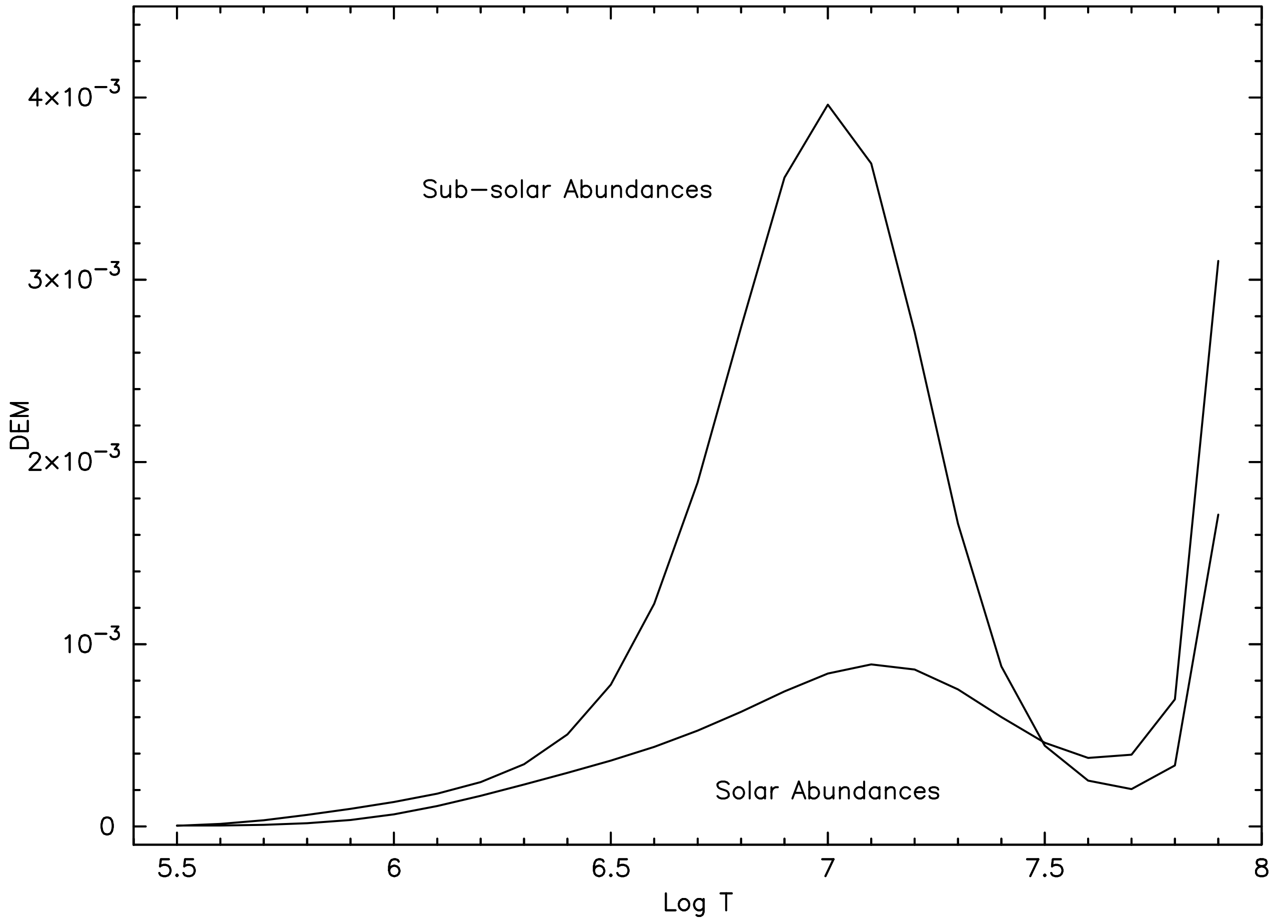

FIG. 9.—Same as Fig. 7, but for Gliese 890

ation with the Castor binary.

The coronal X-ray spectra of YY Gem shows the possible presence of as many as four discrete temperature components. We have examined the possibility that the lowest temperature components here may be contamination from the unresolved quiescent emission due to the A star binary in the Castor system that also contains the YY Gem binary. With *ASCA* it is not possible to extract the quiescent state spectrum of Castor. However, analysis of a spectrum during a flare observed from Castor in the presently analyzed observations showed only low-temperature components (Gotthelf et al. 1994). We have estimated that the total contribution from Castor in quiescence to the YY Gem spectrum during quiescence is at most about 14%. The contributions to the X-ray flux from the 0.26, 0.80, and 1.9 keV components in a three-temperature scenario, on the other hand, are 41.8%, 44.2%, and 14.0%, respectively. Similarly, the contributions to the X-ray flux from the 0.14, 0.57, 0.94, and 2.7 keV components in a four-temperature scenario are 72.7%, 11.7%, 12.6%, and 3%, respectively. The contributions of the lowest temperature components in the quiescent spectrum of YY Gem are, therefore, larger than can be accounted for as contamination from the A star binary in Castor. Most of the low-energy emission appears, therefore, to be from the YY Gem system itself. Whether this low-energy emission is due to additional low-temperature components, or is due to difficulties in estimating abundances in the low-energy region of *ASCA* spectra as seen from the two-temperature fit using the VMEKAL models, cannot be ascertained with good confidence from the present data.

4.2. *Coronal Abundances*

Photospheric abundance measurements are not available for any of the three stars studied here. Based on their membership in the young disk population, the photospheric metal abundances in these stars are expected to be either solar or perhaps slightly supersolar ([Fe/H] $\sim$ 0–0.1). Our analysis of the quiescent X-ray spectra of Speedy Mic and YY Gem, and of the "average" spectrum of Gliese 890, shows that the elemental abundances of the metals are likely (required in the case of YY Gem) to be significantly lower than those found in the solar photosphere. For YY Gem, this is irrespective of the shape of the coronal differential emission measure, as parameterized by either discrete temperature components or by a sixth-order Chebyshev polynomial. This trend has already been seen in coronal X-ray spectra of a number of active stars, e.g., Algol, AR Lac, and β Cet. The pattern of abundances for the individual elements may also be similar in Speedy Mic, Gliese 890, and YY Gem, but higher signal-to-noise spectra of the first two stars are required in order to prove this definitively. The best-fit metal abundances in Speedy Mic, Gliese 890, and YY Gem are, if taken at face value, among the lowest such values yet inferred among active stars studied so far with *ASCA*. For example, the best-fit iron abundance is

TABLE 4

RESULTS FROM JOINT ANALYSIS OF SIS AND GIS SPECTRA OF YY GEM

Abundances Relative to Solar Photospheric[a]	kT (keV)	Emission Measure (10^{52} cm^{-3})	χ^2	Degrees of Freedom
During Quiescence				
Two-temperature models:				
1.0 (fixed)	(0.64, 2.0)	(0.5, 0.6)	539.1	231
$0.12^{+0.02}_{-0.01}$	$(0.30\pm0.02, 0.96\pm0.03)$	$(2.8\pm0.4, 2.6\pm0.2)$	273.7	230
(O = 1.3 ± 0.2, Mg = $0.48^{+0.13}_{-0.11}$, Si = 0.53 ± 0.13, S = $0.7^{+0.3}_{-0.2}$, Ar < 1.4, Ca < 2.8, Fe = $0.29^{+0.06}_{-0.04}$)	$(0.64\pm0.02, 2.3^{+0.3}_{-0.4})$	$(1.32^{+0.14}_{-0.16}, 0.46^{+0.08}_{-0.07})$	198.2	224
Three-temperature models:				
1.0 (fixed)	$(0.25\pm0.03, 0.79\pm0.03, 2.1\pm0.2)$	$(0.44\pm0.02, 0.40\pm0.02, 0.57\pm0.03)$	334.0	229
$0.19^{+0.06}_{-0.03}$	$(0.26\pm0.04, 0.80\pm0.05, 1.9^{+0.7}_{-0.4})$	$(1.8^{+0.5}_{-0.4}, 1.9^{+0.5}_{-0.4}, 0.6\pm0.3)$	214.3	228
Four-temperature models:				
1.0 (fixed)	(0.12, 0.55, 0.89, 2.28)	(3.4, 0.27, 0.28, 0.53)	323.9	227
0.18 ± 0.04	$(0.14\pm0.05, 0.57^{+0.04}_{-0.08}, 0.94^{+0.17}_{-0.10}, 2.7^{+4.0}_{-1.1})$	$(8.1^{+27}_{-1.9}, 1.3^{+0.55}_{-0.45}, 1.4\pm0.4, 0.33^{+0.27}_{-0.20})$	200.9	226
Continuous EM models:				
1.0 (fixed)	[b]	[b]	387.9	228
0.26 ± 0.05	[b]	[b]	286.7	227
During Flare				
Two-temperature models:				
1.0 (fixed)	$(0.69^{+0.07}_{-0.02}, 2.7^{+0.2}_{-0.1})$	$(0.82\pm0.05, 3.1^{+0.10}_{-0.15})$	186.9	196
$0.53^{+0.20}_{-0.17}$	$(0.75^{+0.03}_{-0.07}, 2.65^{+0.20}_{-0.20})$	$(1.6^{+0.6}_{-0.5}, 3.6\pm0.3)$	176.2	195
Three-temperature models:				
1.0 (fixed)	$(0.32^{+0.07}_{-0.07}, 0.84^{+0.03}_{-0.05}, 2.9\pm0.2)$	$(0.40\pm0.12, 0.74\pm0.09, 2.9^{+0.2}_{-0.1})$	159.6	194
$0.60^{+0.21}_{-0.18}$	$(0.32^{+0.09}_{-0.07}, 0.85^{+0.06}_{-0.06}, 2.8^{+0.2}_{-0.2})$	$(0.6^{+0.4}_{-0.2}, 1.2^{+0.5}_{-0.3}, 3.3\pm0.3)$	151.6	193

NOTE.—Errors and upper limits are with 90% confidence based on $\chi^2_{\rm min}+2.71$; distance = 14.7 pc.

[a] Common value of abundances for all the elements in the code, except where stated otherwise.

[b] Sixth-order Chebyshev polynomial.

about 30% of the solar value in the YY Gem quiescent spectrum, comparable to the values inferred from *ASCA* observations of the active binaries AR Lac and Algol. Although the metal abundance estimated during the flare in Speedy Mic showed no change with respect to the value found during the quiescent state, it did show a significant increase during the YY Gem flare. Similar increases in the Fe abundance during flares have been previously reported in Algol and RS CVn binaries (e.g., see Ottmann & Schmitt 1996).

4.3. *Comparison with the X-Ray Properties of Other Late-Type Dwarf Stars*

The X-ray spectral properties measured with *ASCA* are more detailed than those obtained from the earlier, lower resolution measurements. Although the sample of active late-type field stars obtained so far is small, these measurements can still be used to study the effect of fundamental parameters on the X-ray emission characteristics. In Table 5 we present the basic properties and some X-ray characteristics of 10 late-type (G, K, and M) dwarfs that have been published based on *ASCA* observations (Drake et al. 1994; Güdel et al. 1997a; Güdel, Guinan, & Skinner 1997b; Tagliaferri et al. 1997; Mewe et al. 1996, 1998) and the present work. These have been further supplemented with the results from *ROSAT* observations of seven G dwarfs by Güdel et al. (1997b) that were made, inter alia, in order to investigate the saturation in X-ray emission with increasing rotation rate. A similar analysis to the current one by Güdel et al. (1997b) was based mostly on *ROSAT* observations of G-type stars, but lacked rapidly rotating, single stars, including instead rapidly rotating RS CVn binary stars. The latter study used $L_{\rm X}$ as a measure of X-ray emission instead of the luminosity ratio $L_{\rm X}/L_{\rm bol}$ used here. Using the ratio $L_{\rm X}/L_{\rm bol}$, allows us to mix stars of different spectral types but of the same luminosity class and thus to extend the sample to a larger number of stars.

A logarithmic plot of $L_{\rm X}/L_{\rm bol}$ as a function of the rotation period in days for our total sample of 17 stars is shown in Figure 13. Notice that the points would not be well fitted by a simple log-linear fit, as the X-ray emission for those stars with $P < 1$–3 days appears to exhibit a shallower slope than for the longer period stars, consistent with previous findings of activity "saturation" for such short periods. We have tried various functional forms to fit the observed points: for example, we obtain an excellent correlation ($r = -0.941$ for 17 data points) for a relation of the form $\log (L_{\rm X}/L_{\rm bol}) = aP^b$, where $a = -3.38 \pm 0.35$, $b = 0.20 \pm 0.04$, and the variance is 1.26. The best fit with the above functional form has been plotted as a solid line in Figure 13. We have also tried fitting the stars having periods above and below 2 days separately, assuming $\log (L_{\rm X}/L_{\rm bol}) = c$ for the shorter periods, and $\log (L_{\rm X}/L_{\rm bol}) = aP^b$ for the longer periods, and derive $c = -3.19 \pm 0.45$ and a variance of 0.16, and

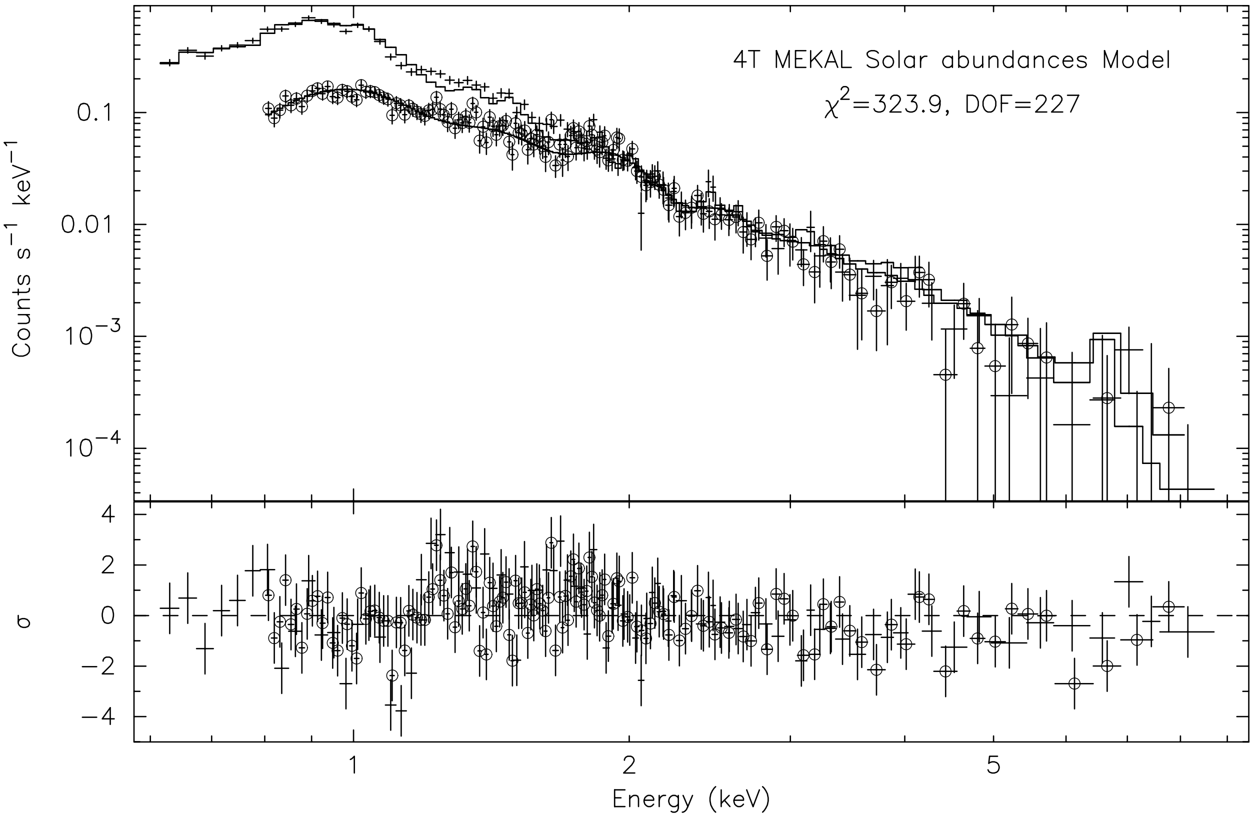

FIG. 10.—Same as Fig. 4, but for YY Gem in its quiescent state. The best-fit four-temperature plasma model with solar abundances, fitted jointly to the SIS and GIS data, is shown as histograms.

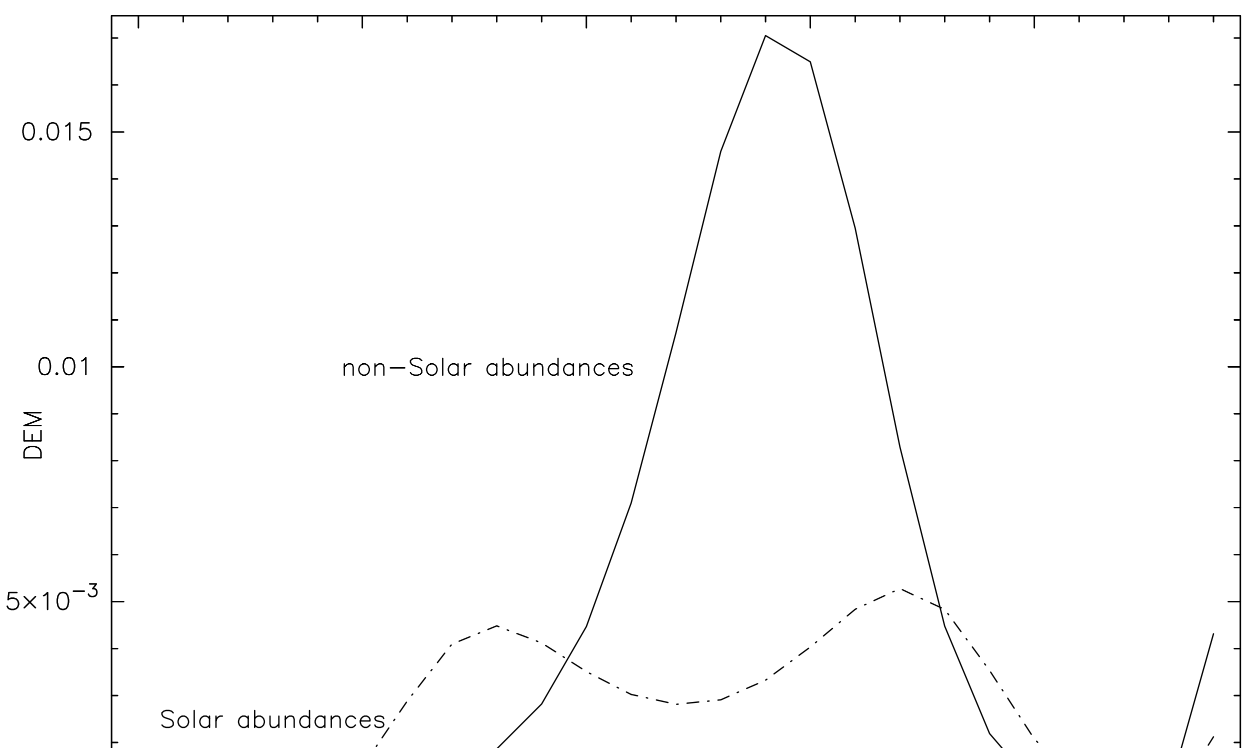

FIG. 11.—Same as Fig. 7, but for YY Gem

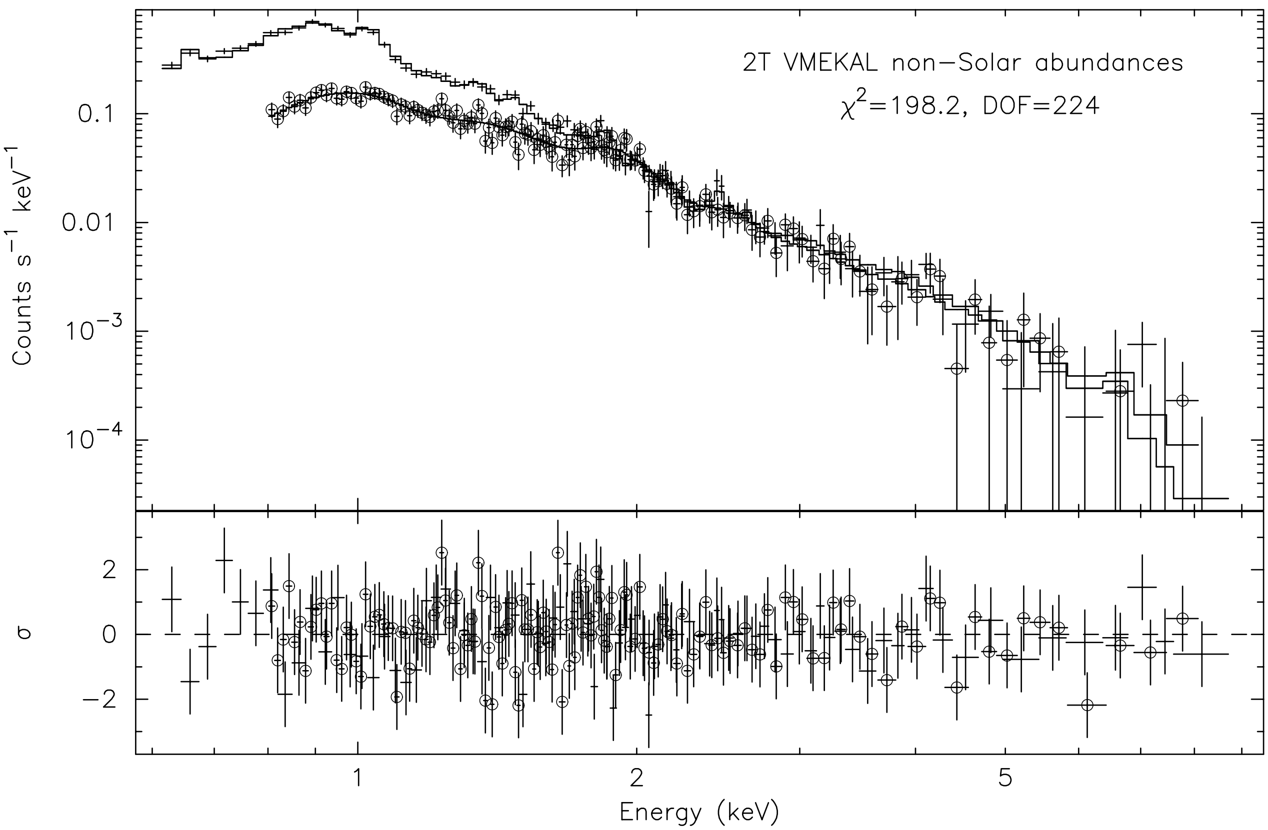

FIG. 12.—Same as Fig. 10, except that the best-fit model here consists of only two temperatures with nonsolar abundances for O, Mg, Si, S, Ar, Ca, and Fe

$a = -3.1 \pm 0.6$, $b = 0.23 \pm 0.07$, and a variance of 0.80, respectively.

The ratio of X-ray to bolometric luminosity is plotted logarithmically as a function of the Rossby number (R_o) in Figure 14. The effect of "saturation" is again obvious in this plot, with the luminosity ratio flattening for values of log R_o smaller than -1. An excellent correlation can again be obtained ($r = -0.893$, $N = 17$) using a slightly more complex functional form $\log\,(L_X/L_{bol}) = a + b\,\log\,R_o + c(\log\,R_o)^2$, where $a = -5.4 \pm 0.3$, $b = -3.3 \pm 1.0$, $c =$

TABLE 5

PARAMETERS OF LATE-TYPE DWARF STARS

Star Name	Spectral Type	$B-V$	Distance (pc)	Period (days)	log R_o	log L_X (ergs s^{-1})	log L_{bol} (ergs s^{-1})	log (L_X/L_{bol})	T_h (keV)	Fe/Fe$_\odot$
				Based on *ASCA* Data						
α Cen	G2 V+K1 V	0.71	1.34	30.0	+0.29	26.96	33.83	−6.87	$0.27^{+0.03}_{-0.03}$	$0.77^{+0.37}_{-0.23}$
π^1UMa	G1.5 Vb	0.62	13.8	4.68	−0.34	28.74	33.51	−4.77	$0.64^{+0.14}_{-0.08}$	$0.41^{+0.24}_{-0.10}$
YY Gem	dM1e	1.49	14.7	0.81	−1.52	29.39	32.45	−3.06	$2.30^{+0.30}_{-0.40}$	$0.29^{+0.06}_{-0.04}$
Speedy Mic......	K2 V	0.93	44.4	0.38	−1.77	29.94	33.01	−3.07	$2.20^{+0.60}_{-0.30}$	$0.21^{+0.08}_{-0.06}$
Gliese 890	dM1.5e	1.40	22.0	0.431	−1.79	29.24	32.27	−3.03	$1.70^{+4.0}_{-0.00}$	$0.17^{+0.11}_{-0.07}$
EK Dra	G0 V	0.63	33.9	2.75	−0.59	29.78	33.54	−3.76	$1.90^{+0.46}_{-0.27}$	$0.99^{+0.30}_{-0.20}$
HN Peg	G0 V	0.59	18.4	4.86	−0.24	28.88	33.66	−4.78	$1.25^{+4.0}_{-0.30}$	$0.72^{+0.40}_{-0.35}$
κ^1Cet	G5 V	0.68	9.16	9.20	−0.18	28.40	33.51	−5.11	$0.70^{+4.0}_{-0.30}$	$0.98^{+0.37}_{-0.23}$
AB Dor	K0–2 IV–V	0.83	15.0	0.517	−1.75	29.93	33.18	−3.25	$1.67^{+0.09}_{-0.09}$	$0.23^{+0.02}_{-0.02}$
HD 35850	F8/9 V	0.55	24.0	1.012	−0.80	30.18	33.68	−3.51	$1.0^{+0.05}_{-0.08}$	$0.25^{+0.03}_{-0.04}$
				Based on *ROSAT* Data						
χ^1Ori	G1 V	0.59	8.66	5.08	−0.22	28.99	33.63	−4.65	...	...
BE Cet	G2 V	0.66	20.4	7.65	−0.22	29.12	33.59	−4.46	...	...
VB 64	G2 V	0.66	46.7	8.7	−0.16	28.90	33.62	−4.72	...	...
β Com	G0 V	0.57	9.15	12.4	+0.22	28.21	33.74	−5.54	...	...
15 Sge	G5 V	0.60	17.7	13.5	+0.17	28.06	33.69	−5.63	...	...
β Hyi	G2 IV	0.62	7.47	28.0	+0.14	27.18	34.14	−6.96	...	...
Sun	G2 V	0.66	1 AU	25.4	+0.30	27.30	33.58	−6.28	...	...

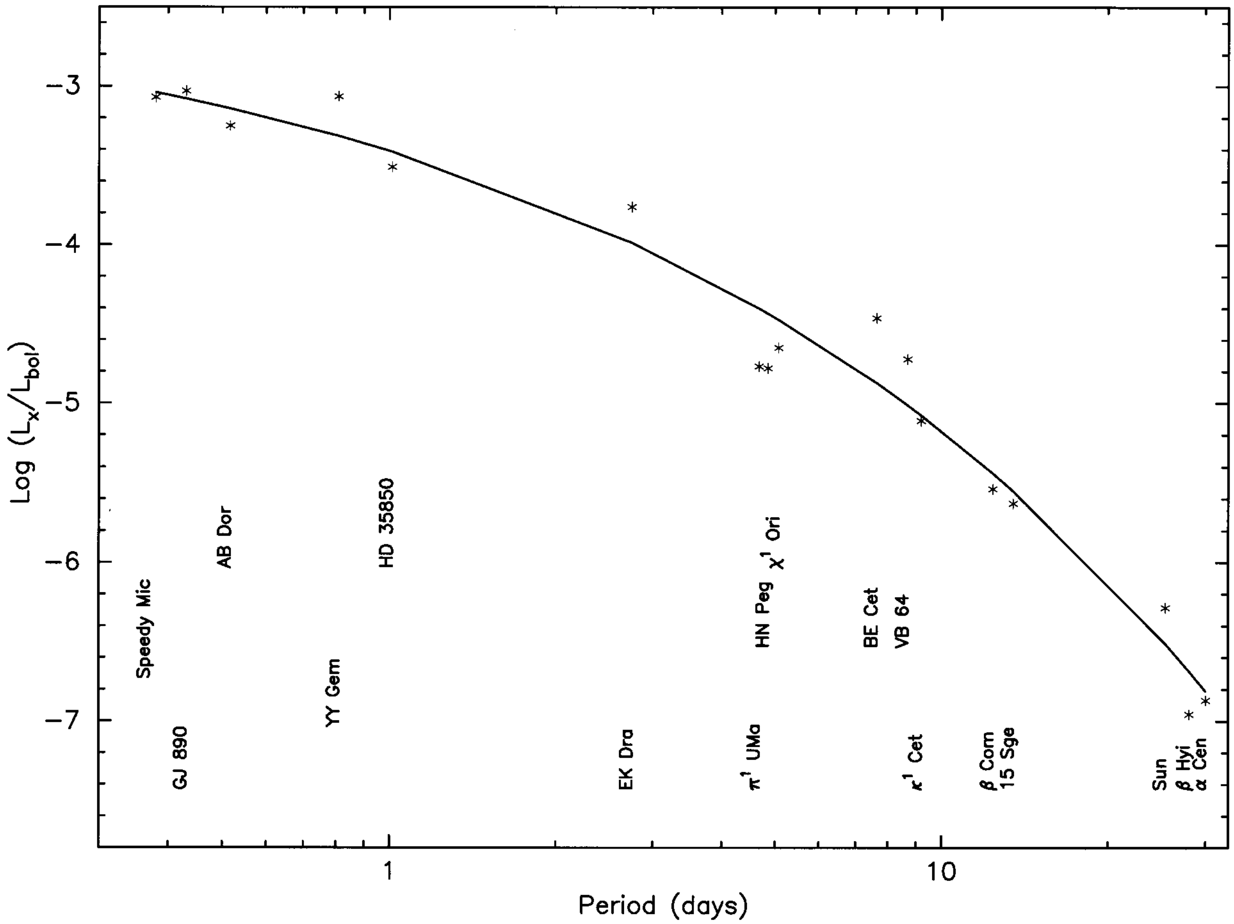

FIG. 13.—Correlation between log (L_X/L_{bol}) and the log of the rotation period of stars in days. The power-law function with the best fit to the data is shown as a solid line.

-1.1 ± 0.6, and the variance is 10.2; this best-fit model is shown as a line in Figure 14.

Based only on the *ASCA*-inferred parameters given in Table 5, we have also examined the dependence of the temperature of the hottest temperature component inferred from the X-ray spectra as a function of L_X/L_{bol} (see Fig. 15). A correlation between the two quantities is clearly present, with the most X-ray–active stars having the hottest temperatures, as has been noted in a number of previous studies. Given the small number of points, we have not attempted to derive a detailed correlation between these two quantities. A similar dependence was seen, for example, by Schmitt et al. (1980), where kT_{max} was found to increase with L_X in a sample that included both dwarfs and giants. The usual interpretation of these correlations is that the stronger dynamo action due to rapid rotation results in enhanced coronal heating that drives the coronal plasma to higher temperatures compared to more slowly rotating stars.

Finally, we consider the possible correlation of the coronal Fe abundances with X-ray activity level (Fe because we believe that its abundance is perhaps the most reliable elemental abundance to be derived from *ASCA* spectra). In Figure 16 we have plotted the values of the coronal Fe abundance relative to the solar value as a function of the ratio of X-ray to bolometric luminosity. The coronal abundance of Fe appears to show an interesting dichotomy: for those stars with log (L_X/L_{bol}) ≤ -3.8, the Fe abundance appears to range between 0.5 and 1.0 times the solar value, while for the more active stars close or at the "saturation" level of -3, the Fe abundance ranges between 0.2 and 0.3 of the solar value. This deficiency of metals has been noted before (e.g., Drake 1996; Schmitt et al. 1996), but there is no generally accepted explanation for the underlying physical causes. Since, for these very active stars, the coronal plasmas have significant emission measure (EM) at temperatures ≥ 1 keV, it is possible either that the processes that control the injection of ionized metals into the coronae are less efficient at these very hot temperatures, or that the hotter plasmas are preferentially depleted of the metals.

Part of the star-to-star scatter may well be due to time variability of the Fe abundance in given stars, particularly during or following stellar flares: studies of X-ray flares observed by *Ginga*, *ASCA*, and *ROSAT* (e.g., Tsuru et al. 1989; Stern et al. 1992; Ottmann & Schmitt 1996; Linsky, Güdel, & Nagase 1997) indicate that, during large flares, the Fe (and other elemental) abundances often appear to increase by a factor of 2 or 3 relative to their preflare values; some studies show that, in the decay phase of the flare, the abundances are slowly decreasing again, presumably back to their preflare values. Thus, the near-solar Fe abundance of the fairly active [log (L_X/L_{bol}) ~ -3.8] G dwarf star EK Dra might have been due to the lingering effects of a large flare that preceded its observation by *ASCA*, and its

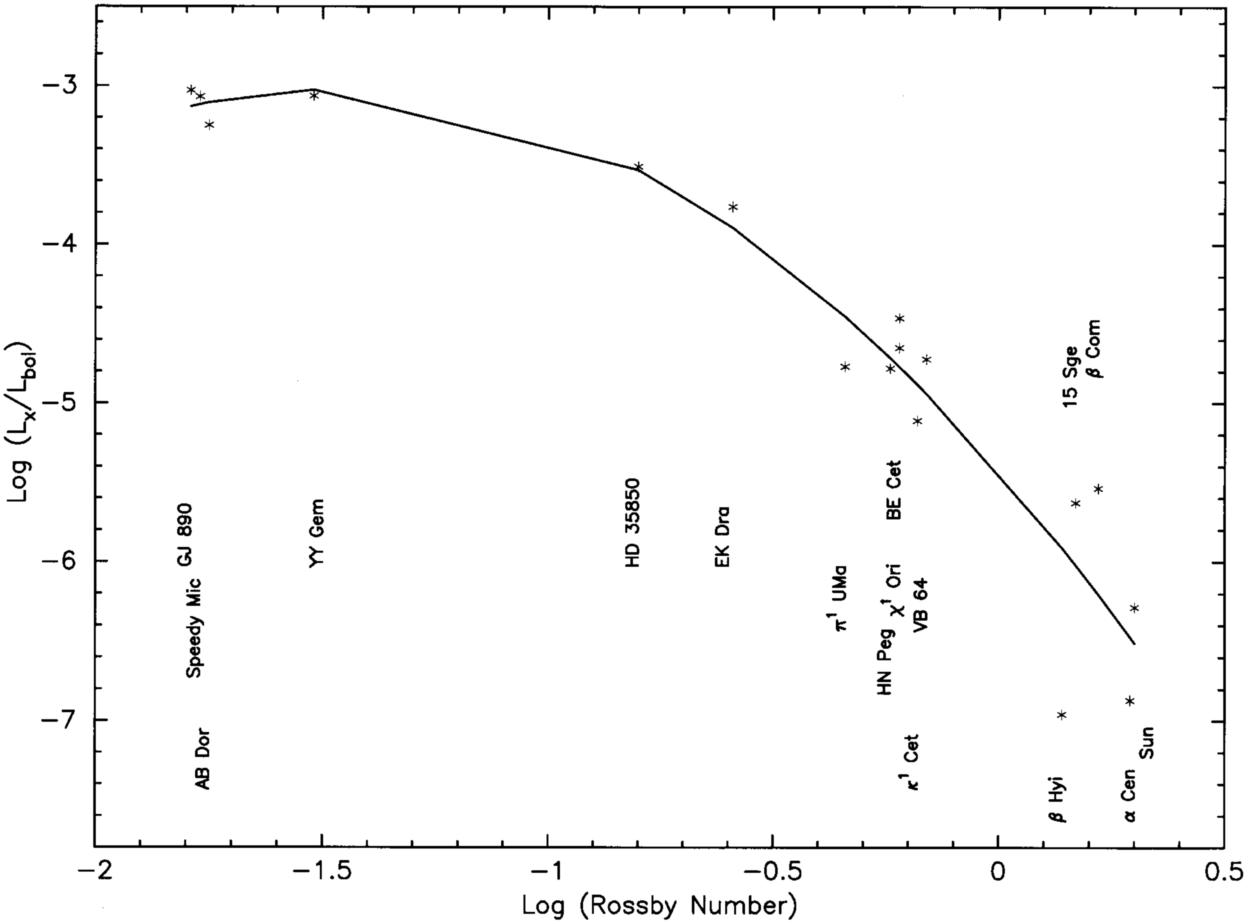

FIG. 14.—Correlation between log (L_X/L_{bol}) and the log of the Rossby number of stars. The quadratic function that is a best fit to the data is shown as a solid line.

"normal" Fe abundance may be much lower. The increased abundance of Fe during the flares, when coronal temperatures are typically higher than during quiescence, is in conflict with the general anticorrelation of these two quantities found for nonflaring stellar coronae, and suggests that a different mechanism, e.g., photospheric or chromospheric "evaporation" of undifferentiated plasma during the flare impulsive phase, is dominant during shorter timescales.

5. CONCLUSIONS

The present X-ray spectroscopic study of Speedy Mic has found that, while subsolar metal abundances do give fits to the data that have lower χ^2_ν values than solar abundance models, the latter models can also give formally acceptable fits, at least for the case where the temperature distribution is represented by a CEM formulation. In the case of Gliese

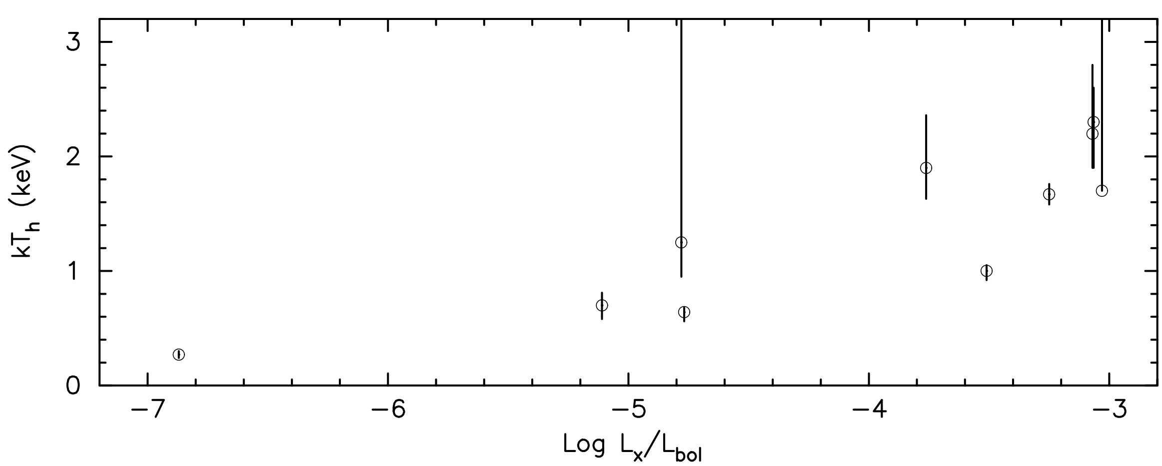

FIG. 15.—Correlation between the highest temperature in the quiescent X-ray emission and log (L_X/L_{bol}) of stars

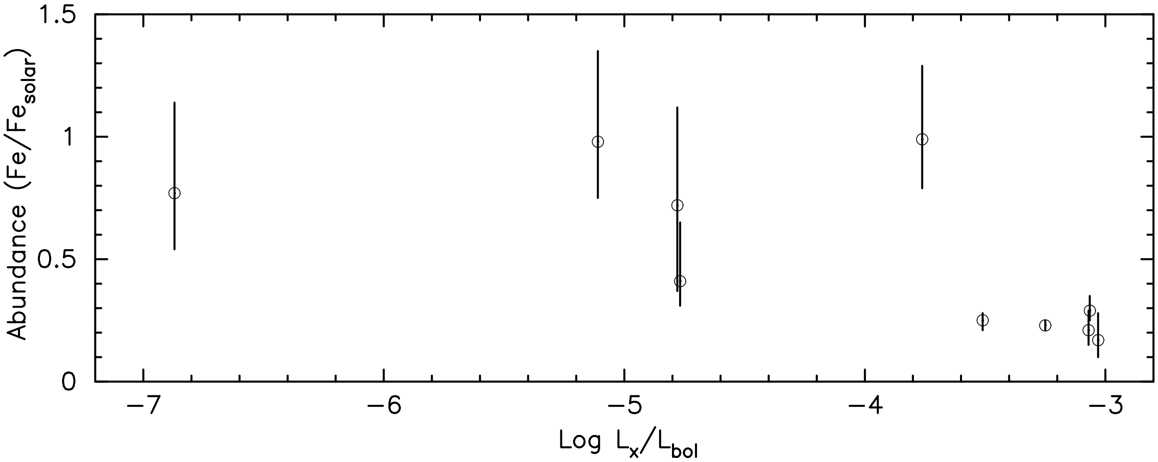

FIG. 16.—Scatter diagram of the abundance of Fe relative to the solar photospheric value vs. log (L_X/L_{bol}) of stars

890, only a single-temperature solar abundance model can be ruled out; two-temperature or CEM models with solar abundances give acceptable fits. In the case of YY Gem, solar abundance models can be ruled out completely irrespective of the temperature structure of the quiescent corona, and all acceptable models require low abundance for metals. Thus, the *ASCA* spectra of all three stars are consistent with their coronae having low levels of metal abundances compared to the solar photospheric values, at least during their quiescent states, although only for YY Gem are the results of the model fitting definitive. The inferred depletion factors of 20%–30% are a little lower than the typical values inferred from the analysis of *ASCA* spectra of subgiant and giant stars of similar X-ray activity (as measured by L_X/L_{bol}), for which coronal Fe abundances of 25%–50% solar are typically found. The latter comparison, if confirmed, might suggest that one of the factors that determines the Fe (and other elemental) abundances in active stellar coronae is the surface gravity. Indeed, in a recent study by van den Oord & Mewe (1999), these authors proposed that the low metal abundances inferred to exist in active stellar coronae are due to density stratification caused by gravitational settling of the hot plasma in coronal loops; this mechanism would seem to be consistent with just such a gravity dependence as is observed.

In agreement with previous studies, we find that the presence of a hard ($T \sim 2.5$ keV) component in the quiescent coronae of these three late-type dwarfs appears to be correlated with their high levels of activity ($L_X/L_{bol} \sim 10^{-3}$). The presence of an unusually strong soft ($T \simeq 0.2$–0.3 keV) component in the corona of YY Gem that is not detected in the other two stars is a priori somewhat suspicious, given that YY Gem is partially confused in the *ASCA* detectors with the nearby multiple A star system α Gem, but we argue that it is likely not due to such contamination. If it is not, then the only other difference between YY Gem and the other two stars is that they are single and it is a binary system: however, such strong soft components have not been inferred from the *ASCA* spectra of other binary stars, and thus it seems implausible that YY Gem's binary nature has anything to do with it. High spatial resolution observations of this interesting wide visual multiple system with *AXAF* may resolve this presently confusing finding.

We wish to thank the entire *ASCA* team for making these observations possible. This research has made use of the FTOOLS and XSPEC software packages provided by the High Energy Astrophysics Science Archive Research Center (HEASARC) of the NASA Goddard Space Flight Center.

REFERENCES

Anders, E., & Grevesse, N. 1989, Geochim. Cosmochim. Acta, 53, 197
Anders, G. J., et al. 1993, MNRAS, 265, 541
Antunes, A., Nagase, F., & White, N. E. 1994, ApJ, 436, L83
Arnaud, K. A. 1996, in ASP Conf. Ser. 101, Astronomical Data Analysis Software and Systems V, ed. G. Jacoby & J. Barnes (San Francisco: ASP), 17
Brickhouse, N. S., Dupree, A. K., Edgar, R. J., Drake, S. A., White, N. E., Leidahl, D. A., & Singh, K. P. 1997, AAS HEAD Meeting
Bromage, G. E., et al. 1992, ASP Conf. Ser. 26, Cool Stars, Stellar Systems, and the Sun, ed. M. S. Giampapa & J. A. Bookbinder (San Francisco: ASP), 80
Byrne, P. B., Eibe, M. T., & Rolleston, W. R. J. 1996, A&A, 311, 651
Byrne, P. B., & McKay, D. 1990, A&A, 227, 490
Cutispoto, G., Kurster, M., Pagano, I., & Rodono, M. 1997, Inf. Bull. Variable Stars, No. 4419
Day, C. S. R., et al. 1995, The ABC Guide to *ASCA* Data Reduction (*ASCA* Guest Observer Facility, NASA Goddard Space Flight Center)
Doyle, J. G. 1987, MNRAS, 224, 1P
Doyle, J. G., & Collier Cameron, A. 1990, MNRAS, 244, 291
Drake, S. A. 1996, in ASP Conf. Ser. 99, Cosmic Abundances, ed. S. S. Holt & G. Sonneborn (San Francisco: ASP), 215
Drake, S. A., Singh, K. P., White, N. E., & Simon, T. 1994, ApJ, 436, L87
Gliese, W. 1969, Catalogue of Nearby Stars (Karlsruhe: G. Braun)
Gotthelf, E. V., Jalota, L., Mukai, K., & White, N. E. 1994, ApJ, 436, L91
Güdel, M., Guinan, E. F., Mewe, R., Kaastra, J. S., & Skinner, S. L. 1997a, ApJ, 479, 416
Güdel, M., Guinan, E. F., & Skinner, S. L. 1997b, ApJ, 483, 947
Jeffries, R. D. 1993, MNRAS, 262, 369
———. 1995, MNRAS, 273, 559
Joy, A. H., & Abt, H. A. 1974, ApJS, 28, 1
Kaastra, J. S., & Mewe, R. 1993, Legacy, 3, 16
Kaastra, J. S., Mewe, R., Liedahl, D. A., Singh, K. P., White, N. E., & Drake, S. A. 1996, A&A, 314, 547
Lemen, J. R., Mewe, R., Schrijver, C. J., & Fludra, A. 1989, ApJ, 341, 474
Liedahl, D. A., Osterheld, A. L., & Goldstein, W. H. 1995, ApJ, 438, L115
Linsky, J. L., Güdel, M., & Nagase, F. 1997, AAS, 191, 44.12
Matthews, L., et al. 1994, MNRAS, 266, 757
Mewe, R., Drake, S. A., Kaastra, J. S., Drake, J. J., Schmitt, J. H. M. M., Schrijver, C. J., Singh, K. P., & White, N. E. 1998, A&A, submitted
Mewe, R., Kaastra, J. S., & Liedahl, D. A. 1995, Legacy, 6, 16
Mewe, R., Kaastra, J. S., White, S. M., & Pallavicini, R. 1996, A&A, 315, 170
Noyes, R. W., Hartmann, L. W., Baliunas, S. L., Duncan, D. K., & Vaughan, A. H. 1984, ApJ, 279, 763
Ottmann, R., & Schmitt, J. H. M. M. 1996, A&A, 307, 813
Pallavicini, R., et al. 1981, ApJ, 248, 279

Pettersen, B. R., Lambert, D. L., Tomkin, J., Sandmann, W. H., & Lin, H. 1987, A&A, 183, 66
Pounds, K. A., et al. 1993, MNRAS, 260, 77
Rao, A. R., & Singh, K. P. 1990, ApJ, 352, 303
Robinson, R. D., et al. 1994, MNRAS, 267, 918
Rucinski, S. M., & Vilhu, O. 1983, MNRAS, 202, 1221
Schmitt, J. H. M. M., Collura, A., Sciortino, S., Vaiana, G. S., Harnden, F. R., Jr., & Rosner, R. 1980, ApJ, 365, 704
Schmitt, J. H. M. M., Stern, R. A., Drake, J. J., & Kürster, M. 1996, ApJ, 464, 898
Singh, K. P., Drake, S. A., & White, N. E. 1995, ApJ, 445, 840
Singh, K. P., White, N. E., & Drake, S. A. 1996, ApJ, 456, 766
Solanki, S. K., Motamen, S., & Keppens, R. 1997, A&A, 325, 1039
Stern, R. A., Uchida, Y., Tsuneta, S., & Nagase, F. 1992, ApJ, 400, 321
Tagliaferri, G., Covino, S., Fleming, T. A., Gagne, M., Pallavicini, R., Haardt, F., & Uchida, Y. 1997, A&A, 321, 850
Tanaka, Y., et al. 1994, PASJ, 46, L37
Tsuru, T., et al. 1989, PASJ, 41, 679
van den Oord, G. H. J., & Mewe, R. 1999, in preparation
White, N. E., et al. 1994, PASJ, 46, L97
Young, A., Skumanich, A., & Harlan, E. 1984a, ApJ, 282, 683
Young, A., et al. 1984b, in Proc. Third Cambridge Workshop on Cool Stars, ed. S. L. Baliunas & L. Hartmann (Berlin, Heidelberg, New York: Springer), 112
Young, A., et al. 1990, ApJ, 349, 608